Interactive comment on "Halo ratio from ground based all-sky imaging" by Paolo Dandini et al.

Response to Anonymous Referee #1

We thank the Referee for many insightful comments and helpful suggestions. We list them below, together with our clarifications and changes to the manuscript, where relevant.

First of all, we must point out that Referee #1, perhaps misunderstanding the purpose of the initial, pre-discussion "access review", provided a similar, detailed review prior to the discussion paper being published. In response the manuscript underwent substantial changes and was then published as the discussion paper. However, in several instances in the latter parts of the present comment the Referee has not taken these changes into account and instead appears to refer to the initial manuscript, which unfortunately is not made available as part of the public discussion. This makes our response and its interpretation difficult and potentially confusing, so to help the readers where this occurs we quote the initial review (labelled "Access review, Reviewer") and response (showing the initial changes and labelled "Access review, Authors", in red) followed by the final reply (labelled "RC1, Authors", in red).

RC1, Reviewer:
• Abstract, Page 2, line 32 and especially Page 6, line 20:
The term "scattering phase function" should not be used in this context. It seems that the analysis in this study is based on the measured brightness distribution of the camera which includes multiple scattering rather than the actual scattering phase function, which is a single scattering property.
Access review, Reviewer:
◦ Page 2, line 31 and especially Page 6, line 19:
The term "scattering phase function" is confusing in this context. It seems that the analysis in this study is based on the measured brightness distribution of the camera which includes multiple scattering rather than the actual scattering phase function, which is a single scattering property.
Access review, Authors:
This is intentional: the corrections applied to the measured radiance are intended to provide an approximation to the unnormalized (1,1) element of the scattering matrix. We use the term phase function as shorthand for this property.
RC1, Authors:
We have responded in the access review. We define our meaning of the term phase function early in the text. However, on page 2, after "*Nevertheless, sky imaging is effective for recording the optical displays sometimes associated with cirrus called halos and for measuring the angular distribution of scattered light*." for greater clarity we continue as follows "*We will henceforth refer to this quantity Scattering Phase Function as the corrections applied to the measured radiance are intended to provide an approximation to the angular dependence of the unnormalized (1,1) element of the scattering matrix*". Further explanation is given in the reply to RC2.

RC1, Reviewer:
· Page 3, line 9:
"...the reflectivity is inversely proportional to the HR." and line 14: "The asymmetry parameter […] is expected to be positively correlated with HR"

These statements are based on observations (Ulanowski et al., 2006; Gayet et al., 2011; Ulanowski et al., 2014) with most HR values < 1, i.e. no 22° halo, which has to be emphasized in this context. Since it is questionable whether differentiating values HR<1 is meaningful at all, the relationship between HR and asymmetry parameter should be explained here first without assumptions:
In general, the reflectivity is primarily determined by the asymmetry parameter which depends on the ice crystal surface roughness and aspect ratio in a U-shaped manner. The HR of the scattering phase function increases for ARs ranging from plates over compact crystals to columns. This implies an ambiguity in the relationship between HR and asymmetry parameter and thus also on the reflectivity.
See

- van Diedenhoven 2012: Remote sensing of ice crystal asymmetry parameter using multidirectional polarization measurements – Part 1: Methodology and evaluation with simulated measurements
- van Diedenhoven 2014: The prevalence of the 22° halo in cirrus clouds
- van Diedenhoven 2014a: A Flexible Parameterization for Shortwave Optical Properties of Ice Crystals

Access review, Authors:
Such ambiguity is indeed expected to exist for geometrically regular, hexagonal ice crystals. However, recent work (see the cited references) indicates that cirrus clouds are dominated by irregular crystals. Ulanowski et al. (2014) show that the halo ratio is inversely proportional to the broadly defined crystal roughness, which in turn is inversely proportional to the asymmetry parameter. As already cited, Gayet et al. (2011) show from in situ observations that the halo ratio is strongly positively correlated with the asymmetry parameter. We now repeat this citation on page 3.
RC1, Authors:
This comment is nearly a verbatim copy of the one given in the access review, too long to be quoted here and to which we believe to have provided adequate response in the initial reply.

· Many abbreviations and acronyms, especially in Sections 2.7 and 3, make the paper difficult to read.
In the following more detailed comments:

1. **Introduction:**

RC1, Reviewer:
The Introduction mainly focuses on cloud detection using all-sky imagers. Are these methods relevant for the presented study?
Access review, Reviewer:

- The Introduction mainly focuses on cloud detection using all-sky imagers. Are these methods relevant for the presented study? I would expect a more detailed review of the literature related to camera observations of halo displays, which is only briefly mentioned (Lynch et al., 1985, Sassen etal. 1994, Forster et al. 2017).

Access review, Authors:
No further literature on all-sky cameras observations of halo displays was found. If we take Forster et al. 2017 as the most recent review, aside from some more amateur-like observing networks of volunteers keeping track of halo phenomena as in (Verschure, P.-P., 1998.) and in (Pekkola, M., 1991), they do not mention any further work in this respect.
RC1, Authors:
We have provided a response in the initial reply to the nearly identical access review. However we can add that it is important to mention the various fields of investigation in which sky imaging finds application: cloud detection is one of these. Also this allows us to

point out widespread use of all-sky cameras and ease with which they could be extended to recording halos and measuring the angular distribution of scattered light.

RC1, Reviewer:
2. **Section 2.2.1:**
◦ Please provide some references for the calibration method using the coordinates of stars.
Access review, Reviewer:
3. **Section 2.2.1:** The description of the calibration method seems a bit incomplete:
◦ Please provide some references for the calibration method, e.g. Kannala and Brandt 2006: "A Generic Camera Model and Calibration Method for Conventional, Wide-Angle, and Fish-Eye Lenses
Access review, Authors:
This is the calibration method for estimating the parameters of the equidistant projection model. This work is not about accurate geometric modelling of real cameras aiming for fine correction of radial and tangential distortions. Described in this section is the calibration procedure to find the camera parameters by assuming the equidistant projection model ($r=f\theta$, "f-theta system"). This assumption is tested in section 2.2.2., and found to be satisfactory.
RC1, Authors:
We have responded to a nearly identical comment in the access review – see above. For clarification, our camera characterization method using the coordinates of stars is not taken from previous work. It is a novel aspect of this study.

RC1, Reviewer:
◦ How does the fit to a bi-cubic function work? Please provide the complete camera model used for the calibration.
Access review, Reviewer:
◦ How does the fit to a bi-cubic function work? Please provide the complete camera model used for the calibration
Access review, Authors:
The only camera model used for the testing of the lens projection is the one identified by eq. 1 and 2, the equidistant projection model.
RC1, Authors:
The bi-cubic function was not used in the final instance for the correction. We have clarified this by replacing the sentences on page 5, lines 25-27: "*This was found by plotting stars using the preliminary projection and determining the difference between the plotted stars and their corresponding background star. The errors as a function of the x, and then y directions were fitted to a bi-cubic function and these added to the coordinates.*" with the following: "*With the preliminary f-theta model so modified the camera parameters were manually adjusted until the difference between the plotted stars and their corresponding background star was minimized.*"

RC1, Reviewer:
◦ Which kind of distortion is corrected – tangential or radial or both?
Access review, Reviewer:
Which kind of distortion is corrected – tangential or radial or both?
Preliminary review, Authors:
There is no distortion correction implemented here. Section 2.2.1 is meant to explain the procedure adopted to measure the camera parameters, namely f, Δ, x_0, and y_0.
RC1, Authors:
For greater clarity we have replaced the phrase in the Abstract "*geometric correction of lens*

distortion" with: "*geometric camera characterization*".
Also, on page 5 we replace "*Finally the empirical scaling factor was applied to the coordinates in the x and y direction to compensate for the distortion created by the lens.*" with "*Finally an empirical scaling factor was applied to the coordinates in the x and y direction. With the preliminary f-theta model so modified the camera parameters were manually adjusted until the difference between the plotted stars and their corresponding background star was minimized*."

RC1, Reviewer:
◦ How many pictures are used for the calibration?
Access review, Reviewer:
◦ How many pictures are used for the calibration?
Preliminary review, Authors:
While one image was used for the camera calibration, for the testing of the lens projection more than 8000 images were processed, roughly one for each point (blue/red dot, fig. 2) of the star/planet's trajectories.
RC1, Authors:
For greater clarity we add on page 5 after: "*Geometric calibration of the camera is done by detecting the position of specific stars and planets in a night-time image and implementing a minimization procedure*." the following sentence: "*This was achieved by using four images, taken at different times of night so that bright stars were available in all quadrants of the image.*"

RC1, Reviewer:
◦ What is the effect of increasing the lens aperture on the accuracy of the geometric calibration?
Access review, Reviewer:
What is the effect of increasing the lens aperture on the accuracy of the geometric calibration?
Access review, Authors:
The tests had to be done with the aperture fully open, so there is no way to determine this effect, if present. However, we do not expect it to be significant. Moreover, the errors that were determined must be the worst case, as agreement with the f-theta projection can be expected to be similar or better for the closed aperture.
RC1, Authors:
A reply was provided in the access review.

RC1, Reviewer:
3. **Section 2.2.2:** The authors state a reprojection error of "mostly <0.1° aside from portions of […] trajectories for which larger discrepancies, up to 0.38°, were observed". How large is the error in the region of interest, i.e. where the 22° halo occurs? Is the accuracy sufficient for this study?
Access review, Reviewer:
4. **Section 2.2.2:** The authors state a reprojection error of "mostly <0.1° aside from portions of […] trajectories for which larger discrepancies, up to 0.38°, were observed". How large is the error in the region of interest, i.e. where the 22° halo occurs? Is the accuracy sufficient for this study?
Access review, Authors:
Such error cannot be stated, as the sun, and hence the halo, can be present at a broad range of zenith angles.

RC1, Authors:
A reply was provided in the access review.

4. **Section 2.5:** Using sun photometer measurements to estimate the vignetting effect of the camera is an interesting approach, but some issues are not discussed.
RC1, Reviewer:
◦ Page 7, line 20: What is the spectral response of the blue channel? The influence of Rayleigh scattering in the blue channel is much stronger compared to the red channel and small deviations in the considered wavelengths might cause larger errors in the radiance distribution. Why not use all 3 (RGB) channels? What is the required accuracy of the vignetting correction?
Access review, Reviewer:
◦ Page 8, lines 3-4: What is the spectral response of the blue channel? The influence of Rayleigh scattering in the blue channel is much stronger compared to the red channel and small deviations in the considered wavelengths might cause larger errors in the radiance distribution. Why not use all 3 (RGB) channels? What is the required accuracy of the vignetting correction?
Access review, Authors:
We use the blue channel as it provides the best spectral match with the sun-photometer operating wavelengths and also because it has a larger quantum efficiency when compared to the green and red channels. Furthermore the quantum response of the red sensor has a larger spectral width.
RC1, Authors:
On page 7 for greater clarity we rephrase "*The blue channel of a clear sky daytime RGB image was extracted, being the best match to a spectral channel of the sun photometer*." as follows: "*The blue channel of a clear sky daytime RGB image was extracted, being the best match to a spectral channel of the sun photometer and having larger quantum efficiency and narrower spectral width of the response than the green and red channels*."

RC1, Reviewer:
◦ Page 7, line 23: "...by neglecting pixels such that z is greater than approximately 20° over the meridian containing the sun...". Why are these pixels neglected?
Access review, Reviewer:
◦ Page 8, line 6: "...by neglecting pixels such that z is greater than approximately 20° over the meridian containing the sun...". Why are these pixels neglected?
Access review, Authors:
Vignetting is assumed to be symmetric under rotations around the camera zenith [(x_0,y_0) or equivalently z=0°]. Hence there is no need to use both halves of the principal plane, the one containing the light source (z<0°) and the one that does not contain the light source (z>0°), to extract the ratio of the two polynomials, one is enough. We decided to use the half such that z>0° and here is why: with respect to fig. 7, pixels such that z <-24° are not taken into account because in this half of the principal plane pixels suitable for measuring the devignetting coefficient are fewer. In fact the camera "sees" the occulting disk while the sun-photometer "sees" the light source, and therefore over the pixels where the occulting disk is located the devignetting coefficient cannot be measured. Nevertheless, pixels such that z<0° but outside the occulting disk region could have been used to take the ratio of the two fitting polynomials. However, this was not done as it was not needed. In fact from the above symmetry argument the devignetting coefficient could be measured using pixels such that z>-24°, as we did.
RC1, Authors:

On page 7 for greater clarity we replace "*by neglecting pixels such that z is greater than approximately 20° over the meridian containing the sun*" with "A*s vignetting is assumed to be symmetric under rotations around the camera zenith, pixels such that z is greater than approximately 20° over the meridian containing the sun were neglected and ... .*"

RC1, Reviewer:

◦ Page 7, line 27: "...the presence of a peak located roughly 8° from the zenith was investigated...To form a correction function symmetric about the zenith, the original curve was "mirrored" about the zenith.." Based on which assumption? Is this peak is related to the camera or the sun photometer data? Was this peak observed at a different time as well?

Access review, Reviewer:

◦ Page 8, line 11: "...the presence of a peak located roughly 8° from the zenith was investigated...To form a correction function symmetric about the zenith, the original curve was "mirrored" about the zenith.." Based on which assumption? Is this peak is related to the camera or the sun photometer data? Was this peak observed at a different time as well?

Access review, Authors:

The vignetting correction is intended to be generic, so that it could be applied to many other sites using the same combination of camera and lens. Since the correction is nearly rotationally symmetric, and we concluded that the residual asymmetry is the outcome of a small misalignment of the sensor, which is likely to vary between cameras, the generic, symmetric correction can be applied to sites where deriving a camera-specific correction is not possible due to the absence of a sun photometer.

RC1, Authors:

For greater clarity at the end of section 2.5 we add the following: "*The vignetting correction so obtained is intended to be generic. Since the correction is nearly rotationally symmetric, and we have concluded that the residual asymmetry is the outcome of a small misalignment of the sensor, which is likely to vary between cameras, the generic, symmetric correction can be applied to sites where deriving a camera-specific correction is not possible due to the absence of a sun photometer.*"

RC1, Reviewer:

◦ Are the measurements interpolated to the same time? How long did the sun photometer scan take?

Access review, Reviewer:

Are the measurements interpolated to the same time? How long did the sun photometer scan take?

Access review, Authors:

The sun-photometer principal plane measurement is performed every hour, over the various wavelengths, one at a time, about 35 s apart.

RC1, Authors:

On page 7 for greater clarity we replace "*The image brightness along the principal plane (containing the zenith and the sun) and the corresponding sun photometer output were compared;*" with the following sentence: "*The sun-photometer measurement along the solar principal plane, performed every hour, over the various wavelengths, one at a time, about 35 s apart, were compared to the corresponding image brightness from the closest camera measurement,;*"

RC1, Reviewer:

◦ Is the vignetting correction determined in the principal plane applied to the whole camera image? If yes, under which assumption?

Access review, Reviewer:
Is the vignetting correction determined in the principal plane applied to the whole camera image? If yes, under which assumption?
Access review, Authors:
See the comment above.
RC1, Authors:
See the comment above.

RC1, Reviewer:
◦ Fig. 6: Why is the calibrated brightness distribution (black dashed line) smoothed compared to the original data (red dashed line)?
Access review, Reviewer:
◦ Fig. 6: Why is the calibrated brightness distribution (black dashed line) smoothed compared to the original data (red dashed line)?
Access review, Authors:
This is due to the fact that the red dashed line is obtained by applying only the geometric correction to the raw data without the inclusion of the background mask. Therefore contamination associated with background objects is not screened out.
RC1, Authors:
At the end of section 2.5 after "*Fig. 6 (black-dashed line) shows the SPF corresponding to the raw image from Fig. 5 when geometric, AM, vignetting and mask corrections are included*." we add the following sentence: "*The latter removes the contamination associated with objects in the field of view, such as trees*."

RC1, Reviewer:
5. Section 2.6: What is the purpose of the air mass correction? Is the applied method of Rapp- Arraras and Domingo-Santos (2011) applicable to cloudy scenes as well? What is the error in this case?
Access review, Reviewer:
5. **Section 2.5:** What is the purpose of the air mass correction? Is the applied method of Rapp-Arraras and Domingo-Santos (2011) applicable to cloudy scenes as well? What is the error in this case?
Access review, Authors:
The purpose of the air mass correction is obvious: it is intended to remove the effect of variable slant path in the single scattering approximation. And the context is thin cirrus, so by definition the scene is cloudy (but the optical depth is low).
RC1, Authors:
The purpose of the air mass correction is simple, as stated at the beginning of section 2.6: the intention is to remove the effect of variable slant path in the single scattering approximation. Otherwise, averaging along lines of constant scattering angle could not be carried out. On page 8 to clarify this we have inserted an explanatory sentence "*With this correction in place averaging of sky brightness along lines of constant scattering angle becomes possible.*" after the text "*the corresponding AM(z).*".

RC1, Reviewer:
6. Section 2.7:
◦ The cirrus BT threshold is based on an optically thick cirrus. 22° halos are only visible in thin cirrus. What is the effect of a decreasing optical thickness on the BT threshold?
Access review, Authors:
We have substantially extended section 2.7, given further detail about the cirrus

discrimination algorithm and highlighted where a further description of it can be found in the literature. Additionally, in Conclusions we have stated that the method has not been tested yet, vis: "*In the future these cirrus discrimination methods should be compared to techniques such as microwave radiometry or lidar which would allow us to assess their relative merit*."

RC1, Authors:

We have responded in preliminary review and have already substantially changed and expanded the manuscript (the changes in section 2.7 comprise 15 lines of text). Testing the BT threshold method, which is only a subsidiary topic in this work, is well beyond the scope of the article, as stated clearly in the manuscript.

RC1, Reviewer:

◦ How sensitive is the presented threshold method on variations of cloud cover in the scene?

RC1, Authors:

See the comment above.

RC1, Reviewer:

◦ The DFA threshold was estimated empirically to 0.02. This value is much lower than the values found by Brocard et al. 2011 (~0.1 for clear sky, ~0.5 for stratiform cirrus, ~1 for broken cirrus), why?

RC1, Authors:

While in Brocard et al. (2011) data were resampled into 5 s bins our data have a time resolution of 1 second. Moreover, while Brocard's FC is calculated over a time interval ranging from 60 to 300 seconds, our FC is fitted over interval lengths ranging from 20 to 60 seconds. In this respect on page 8, line 28, we rephrase "*This threshold was found empirically to be 0.02 on the basis of the DFA output calculated every 20 minutes and over a time scale ranging between 60 and 150 seconds.*" as follows: "*This threshold was chosen empirically to be 0.02 on the basis of the DFA output calculated, unlike by Brocard et al.(2011), every 5 minutes, over data sampled with 1 s resolution and for time intervals ranging between 20 and 60 seconds. The intervals were chosen as the time range over which the DFA function was relatively stable and the slope of the function (the FC) was as sensitive as possible to the presence of clouds.*"

Furthermore, we wish to point out that like in Brocard et al. (2011) the initial analysis step of cumulative summation (integration) of the time series was not carried out. We note that cumulative summation of a self-affine series shifts the FC by +1 (Heneghan and McDarby, 2000), so the threshold applied here would have a value close to 1 if a standard DFA procedure was followed. We place this explanation in the main text.

RC1, Reviewer:

7. Section 3.1:

◦ Page 9, line 28: "...between 8 and 10 am… Over this time window […] the behaviour of the BT and the solar irradiance suggests that the HR increases with the optical thickness τ (see Fig. 10, middle and bottom plots)" This is not clearly visible in Fig. 10. The HR increases from 8:12 until 8:30 am but clearly decreases towards 10 am. How is the optical thickness derived from the displayed data?

Access review, Reviewer:

◦ Page 9, line 15: "...between 8 and 10 am… Over this time window […] the behaviour of the BT and the solar irradiance suggests that the HR increases with the optical thickness τ (see Fig. 10, middle and bottom plots)" This is not clearly visible in Fig. 10. The HR increases

from 8:12 until 8:30 am but decreases towards 10 am. How is the optical thickness derived from the displayed data?

Access review, Authors:

We are discussing optical thickness changes - in this context it is legitimate to consider relative changes in brightness temperature or solar irradiance (the latter opposite in sign), which is done here.

RC1, Authors:

A reply was provided in the access review.

RC1, Reviewer:

◦ Page 9, line 31: Kokhanovsky 2008 showed that the halo contrast is linearly decreasing with increasing optical thickness since molecular and aerosol scattering are neglected. Only **the radiance distribution is increasing up to τ=3 and decreasing for τ>3.**

Access review, Reviewer:

◦ Page 9, line 18: Kokhanovsky 2008 showed that the halo contrast is linearly decreasing with increasing optical thickness since molecular and aerosol scattering are neglected. Only the radiance distribution is increasing up to τ=3.

Access review, Authors:

From Kokhanovsky it follows that there are two regimes with respect to the behaviour of the 22° halo brightness with respect to cloud optical thickness τ. For τ<3 halo contrast increases with τ. Analogously, we observe cirrus whose optical thickness is increasing as testified by the increase of BT and a decrease in solar irradiance, and correspondingly an increase in the halo ratio.

RC1 review, Authors:

The reviewer is confusing our definition of "halo ratio" with Kokhanovsky's definition of "contrast". The reviewer seems to be referring to Fig. 3 of Kokhanovsky's paper showing that "contrast" decreases with τ. However, our definition of the halo ratio differs from Kokhanovsky's definition of "contrast". With respect to the radiance distribution shown in Fig. 2a and 2b of the same paper, page 2, Kokhanovsky states: "*It follows from the analysis of Fig. 2 that basically there are two regimes with respect to the behaviour of the brightness of the halo located around 22° observation angle with respect to the cloud optical thickness. The first effect is the brightening of halo with τ. This occurs till cloud optical thickness of 3 (see Fig. 2a) both in the internal dark halo circle and also in the bright ring. For values of τ>3, the increase in the optical thickness leads to the decrease of halo central ring brightness.*" The behaviour of Kokhanovsky's transmission functions (Fig. 2a and 2b) suggests that, with respect to our definition of the halo ratio, the ratio of the transmitted light at 23° to the transmitted light at 20° increases with τ for τ<3. Analogously, we observe cirrus whose optical thickness is increasing as testified by the increase of BT and a decrease in solar irradiance, and correspondingly an increase in the halo ratio.

RC1, Reviewer:

◦ Page 10, line 2: "Between about 8 and 8:20 am the HR, mostly <1, shows a maximum and a minimum at about 8:06 and 8:12 am, respectively, when a relatively faint 22° halo is visible"

How can the HR be <1 but the image shows a 22° halo? The 22° halo in the image at 8:54 appears brighter than at 8:06 but the HR is smaller. Why? Is this an effect of averaging over the complete 22° halo scattering angle region? If so, the HR might be primarily a measure of cloud fraction in this case.

Access review, Reviewer:

◦ Page 9, line 21: "Between about 8 and 8:20 am the HR, mostly <1, shows a maximum and a

minimum at about 8:06 and 8:12 am, respectively, when a relatively faint 22° halo is visible" How can the HR be <1 but the image shows a 22° halo? The 22° halo in the image at 8:54 appears brighter than at 8:06 but the HR is smaller. Why? Is this an effect of averaging over the complete 22° halo scattering angle region?

Access review, Authors:

Indeed - the reviewer has provided the most likely answer to the question, but it would be speculative to comment further.

RC1, Authors:

As to the original suggestion of the reviewer to use the HR for measuring cloud fraction, it should be pointed out that there are far better ways of doing so. Anyway, this is not the aim of this work. The ultimate goal is deriving reliable HR statistics. The reviewer's scepticism over whether HR is sensitive to the halo status of cirrus is not justified by the overall behaviour of the HR seen over the test cases discussed.

RC1, Reviewer:

8. **Section 3.2:**

Page 11, line 11: "... we conjecture that in order to observe the HR maxima measured for the two cases discussed here a certain minimum fraction of smooth hexagonal ice columns had to be present. If multiple scattering were to be accounted for, such a fraction could be an underestimation of the actual one." The second sentence is now redundant.

Access review, Reviewer:

Page 10, line 31: "According to previous radiative transfer calculations (Forster et al., 2017), we conjecture that in order to observe the absolute HR maxima measured for the two cases discussed here a fraction of at least 20% of smooth hexagonal ice columns was present. If Rayleigh and aerosol scattering were to be accounted for, such a fraction could be an underestimation of the actual one." Why 20%? The simulations in Forster et al. 2017 account for Rayleigh and aerosol scattering.

Access review, Authors:

We changed the manuscript and rewritten this sentence as: "*According to previous radiative transfer calculations (Forster et al., 2017), we conjecture that in order to observe the absolute HR maxima measured for the two cases discussed here a certain minimum fraction of smooth hexagonal ice columns had to be present. If multiple scattering were to be accounted for, such a fraction could be an underestimation of the actual one*."

RC1, Authors:

We removed the redundant phrase "*If multiple scattering were to be accounted for, such a fraction could be an underestimation of the actual one*."

RC1, Reviewer:

9. Conclusions:

◦ Page 11, line 29/30: "Overall the HR is shown to be sensitive to the halo status of cirrus as it is well correlated with halo visibility." Can you provide a quantitative statement?

Access review, Reviewer:

◦ Page 11, line 17: "Overall the HR is shown to be sensitive to the halo status of cirrus as it is well correlated with halo visibility." Can you provide a quantitative statement?

Access review, Authors:

Unfortunately, we do not know of a quantitative measure of halo visibility - it is a subjective one.

RC1, Authors:

We repeat our initial reply.

RC1, Reviewer:

◦ Page 12, line 3-9: Discrimination between cloud and clear sky seems to work well using the halo ratio alone, without additional DFA threshold test. Discrimination between cirrus and broken cumulus or other clouds seems necessary. How (well) does it work?

Access review, Reviewer:

◦ Page 11, line 24-30: Discrimination between cloud and clear sky seems to work well using the halo ratio alone. Discrimination between cirrus and broken cumulus or other clouds seems necessary. How does the presented method perform compared to the methods presented in the Introduction for cloud type discrimination and halo detection? (e.g. Shields et al. 2013, Forster et al. 2017)

Access review, Authors:

It is not possible to answer this question - we have pointed out in the conclusions (page 12 lines 3, 4 and 5) that such method "*should be compared to techniques such as microwave radiometry or lidar which would allow us to assess its relative merit.*"

RC1, Authors:

See the access review Authors' response here and "Section 2.7" above - the same manuscript modifications apply. Thus the required changes are already in the current version of the manuscript.

RC1, Reviewer:

◦ How does the presented method perform compared to the methods presented in the Introduction for cloud type discrimination and halo detection? (e.g. Shields et al. 2013, Forster et al. 2017)

Access review, Reviewer:

How does the presented method perform compared to the methods presented in the Introduction for cloud type discrimination and halo detection? (e.g. Shields et al. 2013, Forster et al. 2017)

Access review, Authors:

See the comment above.

RC1, Authors:

See the access review Authors' response here and "Section 2.7" above - the same manuscript modifications apply. The required changes are already in the current version of the manuscript.

RC1, Reviewer:

◦ Page 12, line 26: "We argue that when the 22° halo was visible a percentage of at least 20% of regular ice crystals had to be present if molecular, aerosol and multiple scattering in addition to surface albedo are accounted for, together contributing to a reduction of the halo contrast." What is the basis of this argument? Please explain.

Access review, Reviewer:

◦ Page 12, line 14: "We argue that when the 22° halo was visible a percentage of at least 20% of regular ice crystals had to be present if molecular, aerosol and multiple scattering in addition to surface albedo are accounted for, together contributing to a reduction of the halo contrast." What is the basis of this argument? Please explain.

Access review, Authors:

Radiative transfer calculations (Forster et al. 2017) not accounting for multiple scattering suggest that roughly 20% is the fraction of smooth particles needed for the halo to be visible. Given that the all-sky camera does not screen out the effect of multiple scattering, it is reasonable to think that such fraction could be larger, as multiple scattering reduces halo visibility.

RC1, Authors:
Page 12, line 26, we replaced the following sentence "*We argue that when the 22° halo was visible a percentage of at least 20% of regular ice crystals had to be present if molecular, aerosol and multiple scattering in addition to surface albedo are accounted for, together contributing to a reduction of the halo contrast.*" with: "*We argue that when the 22° halo was visible a percentage of at least 20% of regular ice crystals had to be present.*"
This is based on sensitivity studies of light scattering simulations (Forster et. al., 2017) showing (see Fig. 11 of Forster et. al.) that HR>1 is associated to smooth crystal fraction larger than 20%, as already cited (end of section 3).

RC1, Reviewer:
◦ Page 12, line 28: "We have also conjectured that when the HR reached its absolute maxima the fraction of such pristine crystals is likely to have been much larger than 20%." See previous comment.
"The remaining fraction could have been composed of irregularly shaped, complex, rough or small ice crystals." In Sections 3.1 and 3.2 fluctuations of the HR are explained only by variations of the cloud optical thickness, now the argument is based on the ice crystal microphysical properties. This is not consistent.
Access review, Reviewer:
◦ Page 12, line 16: "We have also conjectured that when the HR reached its absolute maxima the fraction of such pristine crystals is likely to have been much larger than 20%. The remaining fraction could have been composed of irregularly shaped, complex, rough or small ice crystals." In Sections 3.1 and 3.2 fluctuations of the HR are explained only by variations of the cloud optical thickness, now the argument is based on the ice crystal microphysical properties. This is not consistent.
Access review, Authors:
We do not understand the Reviewer's objection: the halo ratio depends on both optical thickness and microphysical properties. We make this point several times in the text. Perhaps the Reviewer was confused by the emphasis in the observation sections on optical thickness, as we have its indirect measures (via solar irradiance, BT etc.) hence we can draw conclusions on its impact on HR, while the later discussion also takes in modelling results that account for microphysics.
RC1, Authors:
We can only repeat our initial response.

RC1, Reviewer:
◦ Page 13, line 1: should be "...e.g. the presence of sun dogs and the 46° halo indicates the presence of aligned plates and **randomly oriented hexagonal crystals**, respectively."
Access review, Reviewer:
◦ Page 12, line 23: "...e.g. the presence of sun dogs and the 46° halo indicates the presence of aligned plates or solid columns, respectively." The 46° halo is formed by randomly oriented hexagonal crystals, not aligned solid columns.
Access review, Authors:
We did not intend to say that the 46° halo is caused by aligned columns, but solid columns. Perhaps our meaning will be clearer if we replace the conjunction "or" with "and".
It now reads: "*Furthermore, by extending the method to additional halo displays further information on ice crystal geometry could potentially be obtained - e.g. the presence of sun dogs and the 46◦ halo indicates the presence of aligned plates and solid columns, respectively.*"
RC1, Authors:

We have already replied to this and changed the phrasing accordingly; moreover we believe our statement to be more precise than the suggested one.

RC1, Reviewer:

◦ Page 13, line 3: "The utilisation of the all-sky cameras to transform the measured light intensity into the scattering phase function and, on a limited extent, the cirrus detection algorithm, are the particularly novel aspects of this work; this has not been done previously to the best of our knowledge." The term "cirrus detection algorithm" appears only in the Abstract and Conclusions. Where is this algorithm explained? The method described in Section 2.7 is not new and was already published by Brocard et al., 2011.

Access review, Reviewer:

◦ Page 12, line 24: "The utilisation of the all-sky cameras to transform the measured light intensity into the scattering phase function and, on a limited extent, the cirrus detection algorithm, are the particularly novel aspects of this work; this has not been done previously to the best of our knowledge." Which cirrus detection algorithm? The used method was already described in Brocard et al., 2011.

Access review, Authors:

Our cirrus detection algorithm does not rely solely on the method of Brocard et al. but includes thresholding of the level, as opposed to the fluctuations, of brightness temperature.

RC1, Authors:

Section 2.7 has already been substantially extended, further detail about the cirrus discrimination algorithm was given and relevant literature cited, as described in "Section 2.7" above. The Reviewer appears not to have re-read the manuscript.

RC1, Reviewer:

◦ Page 13, line 10: " The combined use of these two methods, allows relatively inexpensive halo observations and the retrieval of information pertaining to ice particles size and texture." How can particle size an texture be retrieved?

Access review, Reviewer:

◦ Page 12, line 31: " The combined use of these two methods, allows relatively inexpensive halo observations and the retrieval of information pertaining to ice particles size and texture." How can particle size an texture be retrieved?

Access review, Authors:

We are not saying that particle size and texture can be retrieved, certainly not individually.

RC1, Authors:

We stand by our initial response.

Interactive comment on “Halo ratio from ground based all-sky imaging” by Paolo Dandini et al.

Response to Anonymous Referee #2

We thank the Referee for many insightful comments and helpful suggestions. We list them below, together with our clarifications and changes to the manuscript.

Major points:

- The term "scattering phase function" is misleading, as I already mentioned in the quick review. The scattering phase function a clearly defined single scattering property, in particular the probability of scattering into a certain direction. What the authors determine here is a normalised radiance distribution. In case of optically very thin clouds (tau«1, single scattering), the radiance distribution would be close to the scattering phase function if there was no additional molecular scattering. Please avoid the term because it is misleading!
Authors: We do not claim that what we observe is due solely to cirrus, and a phase function remains a phase function even if it is due to a mix of scattering components. It is appropriate to acknowledge that in some cases the observations depart from the single scattering assumption. However, a term like "sky radiance" is not suitable. This is because our results focus on radiance that is corrected for the relative airmass contribution, so is not simply sky brightness. Our use of the term phase function is intentional: the corrections applied to the measured radiance are intended to provide an approximation to the angular dependence of the unnormalized (1,1) element of the scattering matrix. We use the term phase function as shorthand for this property. There is no other term in common use that we are aware of that describes the angular dependence of scattering in this context. We define the meaning of our usage of the term phase function early in the text.
However, for greater clarity, after “*Nevertheless, sky imaging is effective for recording the optical displays sometimes associated with cirrus called halos and for measuring the angular distribution of scattered light.*” we continue as follows “*We will henceforth refer to this quantity Scattering Phase Function as the corrections applied to the measured radiance are intended to provide an approximation to the angular dependence of the unnormalized (1,1) element of the scattering matrix.*”.

- After the two case studies, I am not sure if the brightness temperature fluctuation threshold provides any useful information. Nearly all shown data points are clearly above the threshold. It would be good to see examples where the values are actually below the threshold.
Authors: Cirrus discrimination is only a subsidiary topic of the present article, the main aim being the retrieval and the behaviour of the halo ratio. Therefore, for brevity, we focus almost exclusively on cloudy skies. Brightness temperature fluctuation as a means to detect cirrus has been the subject of the previous studies.

- Conclusions, page 12, line 26: Where do the numbers (20%) concerning smooth crystal fractions come from? I do not see any evidence in the manuscript, neither any reference. If there is no quantitative evidence, please remove the statement.
Authors: This is based on sensitivity studies of light scattering simulations (Forster et. al., 2017) showing (see Fig. 11 of Forster et. al.) that HR>1 is associated to smooth crystal fraction larger than 20%, as already cited (end of section 3).

- How was the halo ratio determined from the images? Maybe I missed it, but it isn't clear to me if the average over the full circle around the transformed image center was taken, or if only a sector was used, or ... And how does the (admittedly small) angular error affect the halo ratio?

Authors: The halo ratio is determined from the phase function, as already described in the introduction and then extended at the beginning of section 3 with the definition of scattering angles in use. So the Reviewer's question boils down to how the phase function is obtained; this is described at the beginning of section 2.3, as follows: "*The SPF is obtained by averaging the image brightness over pixels which are equidistant from the light source in terms of scattering angle*", and then reinforced at the end of this section with reference to the example image as "*The interpolated image is ultimately used to calculate the brightness as a function of the scattering angle"* For greater clarity we now insert at the end the words "*by averaging over the entire azimuth angle range*."

As to the effect of the angular error on the halo ratio, we have not studied this aspect, beyond determining that the angular error is small, as the reviewer states.

Minor points:

Page 2, line 20: This is not really a sentence and the level of detail could be reduced, since it is anyway not sufficient to understand the technique without having to read the referenced paper.

Authors: The following sentence "*Field images, a red, a blue and a red and a blue trimmed with neural density were calibrated for the non-linearity of the basic sensor and for differences in the pass bands of the spectral filters and then used to obtain the corresponding blue to red ratio images before a threshold was set for determining the presence of thin clouds*." has been as modified as follows: "*Field images were used to obtain the corresponding blue to red ratio images before a threshold was set for determining the presence of thin clouds*.".

Page 3, line 23: "previous" findings are contrasted to more recent results. However, these two papers describe observations in completely different locations on the globe which might be one cause for differences.

Authors: While these observations are from different geographic locations they both have been recorded in the northern-hemisphere for a mid-latitude scenario. Here we are not trying to give reasons as to why different studies show different results. We only want to stress that differences exist and should be resolved. Here we propose enabling this by the introduction of an inexpensive and easy to implement technique.

Page 4, line 3: Since the reader might now be familiar with the details of image vignetting at this point in the text, this section might be moved after the "all-sky-camera" section.

Authors: we think that there is a need for a short introduction to the instrumentation used, prior to a more detailed description of the cameras.

Page 4, line 16: What are these "2.52%"? Fraction of the solid angle? Please define.

Authors: We are referring to area only in this sentence: 2.52% is the fraction of the area of the sky. But to remove ambiguity we rephrase the end of the sentence to read: "*2.5% cut off at the top and at the bottom*" (note that now 95%+2.5%+2.5%=100% exactly).

Page 4, line 21: I am not sure how many readers are still familiar with kbaud. One might use kbit/s instead.
Authors: we have altered this as suggested.

Page 4, line 25: The shadow disk for the daytime camera is meant to reduce stray light. Isn't the same necessary for the night time camera? The moon is certainly six orders of magnitude darker than the sun, but the lunar halo is as well. Or in other words, the ratio of the brightness lunar halo / moon should be the same as the ratio solar halo / sun. The straylight problem should be the same during day and night.
Authors: The measurements of the halo ratio use the daytime camera, and the night-time camera provided only star positions for testing the lens projection. Hence we show the shade used for the daytime camera only. The referee is probably correct that the stray light effect should be accounted for at night too, but we do not suggest otherwise!

Page 5, line 27: Could you provide the formula of the bi-cubic function and the order of magnitude of the deviation from the ideal camera model? From statements in the following section I infer that it was actually not used? If so, why mention it at all?
Yes, it is correct that the bi-cubic function was not used in the final instance for the correction. To remove the ambiguity, we have replaced the sentences on page 5, lines 25-27:
"*This was found by plotting stars using the preliminary projection and determining the difference between the plotted stars and their corresponding background star. The errors as a function of the x, and then y directions were fitted to a bi-cubic function and these added to the coordinates.*"
with the following:
"*With the preliminary f-theta model so modified the camera parameters were manually adjusted until the difference between the plotted stars and their corresponding background star was minimized.*".

Page 6, line 8: I assume, the test image here was different from the one in the previous section which was used for the geometric calibration?
Authors: Yes, they are not the same. Fig. 2 shows the image used for the testing of the lens projection model, as stated 3 lines later.

Page 7, line 16: Could you briefly (one sentence) explain what vignetting is and how it is caused?
Authors: additional text "*Optical and natural vignetting are associated with smaller lens opening for obliquely incident light and the* $\cos^4$ *law of illumination falloff, respectively, both inherent to any lens design (*Ray, 2002;*"* has been inserted after "*... in particular wide-angle and ultra-wide-angle lenses like fisheye lenses*", with the new reference: Ray, S. F.: Applied photographic optics, Focal Press, Oxford, 2002.

Page 7, line 24: Explain acronym LOWESS
Authors: we have inserted the explanatory text "(*Locally Weighted Scatterplot Smoothing*)".

Page 7, line 27: with "the presence of a peak located roughly 8°" you mean that the maximum of the function is at 8° rather than at 0° where you would expect it?
Authors: Yes, that is correct. To clarify the meaning, we have replaced the text with "*the shift of the maximum from the zenith to the position at roughly 8°*".

Page 8, line 1: Could you please explain why the average between the original and the mirrored curve was used, rather than shifting the curve by 8°?
Authors: As is explained later in the text, the purpose is to form a rotationally symmetric devignetting function, centred on the zenith.

Figure 8, caption: This is confusing and contradicts the text: The caption says "stretched", while the curve is obviously shifted. The text on the other hand says "mirrored" rather than shifted.
Authors: The red curve is not shifted, it is indeed stretched, i.e. the value at the margin of the image is kept constant. To achieve that, the curve is simply mirrored about the zenith, as explained in the text.

Page 8, line 8: The purpose of the airmass correction is not clear to me. Is it to make the brightness distribution more "flat"?
Authors: The purpose of the air mass correction is simple, as stated at the beginning of section 2.6: the intention is to remove the effect of variable slant path in the single scattering approximation. Otherwise, averaging along lines of constant scattering angle could not be carried out. To clarify this, we have inserted an explanatory sentence "*With this correction in place averaging of sky brightness along lines of constant scattering angle becomes possible.*" after the text "*the corresponding AM(z).*".

Page 8, line 19: To assume single scattering the slant optical thickness has to be smaller than 1. For a viewing zenith angle of 70° the slant optical thickness would be about three times the vertical optical thickness, and thus the assumption of single scattering would only be true for clouds with vertical optical thickness smaller than 0.3. I am sure many of the observed cirrus clouds had a larger optical thickness. Also, the vertically integrated Rayleigh optical thickness in the blue is about 0.2 which adds to the cirrus optical thickness. This once more confirms that you don't observe the scattering phase function but the sky radiance which is caused by cloud scattering plus molecular scattering.
Authors: Please see the first comment for our explanation and justification of our use of the term phase function. Concerning optical thickness, the Reviewer is correct that in some instances a departure from the single scattering approximation would have occurred, especially at higher zenith angles. But the purpose of this work was not to obtain the single scattering phase function in the strict sense. The aim was to retrieve the halo ratio, and for that purpose a number of corrections was applied, one of which was the airmass correction, which implicitly assumed the single scattering approximation. So it is a compromise, but one that allowed us to average sky brightness over most of the sky, with the advantages that this brings.

Page 8, line 27: How was the threshold determined empirically? From "manually" deciding if an image is cloud/cloudless and looking at the corresponding fluctuation?
Authors: With reference to Dandini (2016) and Fig. 3.19 and 3.20 therein, the DFA algorithm was applied to one year of continuous BT data. Then the all-sky images associated with minima of the fluctuation coefficient were selected. From this subset of images a manual cloud screening was done by visual inspection before taking the average FC, which was found to be 0.02. For additional explanation, we now add after "*The DFA algorithm was applied to one year of data and the corresponding FC time series was averaged over clear sky periods to set the DFA threshold.*" the following sentence: "*This was obtained after manual cloud screening of images associated with minima of the fluctuation coefficient.*"

Page 9, line 8: With "irradiance due to the direct emission of cirrus corrected for the atmospheric attenuation" you actually mean after correction to brightness temperature assuming Stephan-Bolthmann? The large deviation from -38°C results from the fact that your broadband instrument integrates over water vapor absorption as well as the atmospheric window? At first glance I expected it to be closer to -38°C, but that would only be the case for a narrowband instrument measuring in the atmospheric window.

Authors: The Stephan-Boltzmann does not apply to this case as we approximate the narrow-band spectral response of the pyrometer KT15.85 (in the atmospheric window) to be monochromatic, at the central wavelength.

As to the text "*…the irradiance due to the direct emission of cirrus corrected for the atmospheric attenuation, was obtained (see Fig. 10 and 12, middle plot, black dashed line)*." it means that the direct cirrus emission is attenuated by the water vapour layer below the cloud before entering the instrument; this quantity is then added to the modelled water vapour direct emission and the final result is turned into brightness temperature by inverting Planck's law. The large deviation of the Ci threshold from -38° is mainly due to the fact that the model accounts also for direct emission from the water vapour layer below the cloud.

For greater clarity we have rephrased the text to read *"….the irradiance due to the direct emission of cirrus corrected for the atmospheric attenuation and emission was obtained, and converted to brightness temperature by inverting Planck's law (see Fig. 10 and 12, middle plot, black dashed line).*"

Halo ratio from ground based all-sky imaging

Paolo Dandini[1], Zbigniew Ulanowski[1], David Campbell[1], and Richard Kaye[2]

[1]School of Physics Astronomy and Mathematics, University of Hertfordshire, Hatfield, AL10 9AB, UK
[2]School of Engineering and Technology, University of Hertfordshire, Hatfield, AL10 9AB, UK

Correspondence to: Z. Ulanowski (z.ulanowski@herts.ac.uk)

Abstract. The halo ratio (HR) is a quantitative measure characterizing the occurrence of the 22° halo peak associated with cirrus. We propose to obtain it from the scattering phase function (SPF) derived from all-sky imaging. Ground based fisheye cameras are used to retrieve the SPF by implementing the necessary image transformations and corrections. These consist of geometric ~~correction of lens distortion~~ camera characterization by utilizing positions of known stars in a camera image, transforming the images from the zenith-centred to the light-source-centred system of coordinates, correcting for the air mass and for vignetting, the latter using independent measurements from a sun photometer. The SPF is then determined by averaging the image brightness over the azimuth angle and the HR by calculating the ratio of the SPF at two scattering angles in the vicinity of the 22° halo peak. In variance from previous suggestions we select these angles to be 20° and 23°, on the basis of our observations. HR time series have been obtained under various cloud conditions, including halo cirrus, non-halo cirrus and scattered cumuli. While the HR measured in this way is found to be sensitive to the halo status of cirrus, showing values typically >1 under halo producing clouds, similar HR values, mostly artefacts associated with bright cloud edges, can also be occasionally observed under scattered cumuli. Given that the HR is an ice cloud characteristic, a separate cirrus detection algorithm is necessary to screen out non-ice clouds before deriving reliable HR statistics. Here we propose utilizing sky brightness temperature from infrared radiometry: both its absolute value and the magnitude of fluctuations obtained through detrended fluctuation analysis. The brightness temperature data permits the detection of cirrus in most but not all instances.

1 Introduction

Cirrus clouds are composed of ice crystals. It is well established that because of their high global coverage their impact on the Earth's climate is significant and to quantify it the microphysical and radiative properties of cirrus have to be better represented in atmospheric models (Baran, 2012). This is not trivial as the ice crystals which compose cirrus can take on a wide variety of non-spherical shapes and have size ranging from a few microns up to over a millimetre, making detailed characterization of cirrus difficult and light scattering by cirrus highly challenging to model. Furthermore, as cloud forcing must be quantified from solar to thermal wavelengths, a correct parameterization of cirrus properties is necessary over the same spectrum. To characterize cirrus we propose here the use of sky imaging.

Sky imaging finds application in determining fractional cloud cover (Johnson and Hering, 1987; Long and DeLuisi, 1998; Slater et al., 2001; Long et al., 2001; Berger et al., 2005; Kassianov et al., 2005; Cazorla et al., 2008b), macrophysical cloud

properties such as cloud brokenness, distribution, number and uniformity (Shields et al., 1997; Kegelmeyer, 1994; Long et al., 2006), in assessing the impact of cloud cover on surface solar irradiance (Pfister et al., 2003), in estimating cloud base height either from low-cost digital consumer cameras (Seiz et al., 2002; Janeiro et al., 2010) or by means of paired whole sky cameras (Lyons, 1971; Rocks, 1987; Allmen and Kegelmeyer, 1996), in cloud detection and classification (Calbó and Sabburg, 2008; Heinle et al., 2010; Ghonima et al., 2012), in short term weather forecasting (Chow et al., 2011), in characterizing aerosol (Cazorla et al., 2008a) and in determining cloud-free lines of sight (Shaklin and Lund, 1972; Shaklin and Lund, 1973; Lund, 1973; Lund et al., 1980). Sky imaging is not new in the field of cirrus investigation as testified by previous works on measurements of the 22° halo intensity from photographic photometry (Lynch et al., 1985), on the effects of ice-crystal structure on halo formation (Sassen et al., 1994) and on the characterization of cirrus through a combination of polarization lidar and photographic observations of cirrus optical displays (Sassen et al., 2003). Yet sky imaging in itself is a poor technique for detecting cirrus, in particular when optically thin. Misdetection of thin clouds and limitations in cloud type classification are the major disadvantages of ground based sky cameras (Calbó et al., 2008; Heinle et al., 2010). This is true in particular within a scattering angle of 20° as forward scattering from thin cirrus or boundary layer haze and blooming of the camera sensor can give rise to artefacts that make the sky around the sun appear as if it is cloudy even if it is not (Tapakis et al., 2013). A solution to this issue consists in using sun tracking occulting masks to prevent direct sun light from interfering with the image (Martinez-Chico et al., 2011). To overcome the problem of detecting cloud presence near the sun's location statistical approaches, using the mean and standard deviation of cloud coverage, have also been proposed (Pfister et al., 2003; Long, 2010). One of the first thin cloud algorithms to be developed (Shield et al., 1990), was based on the ratio Red/Blue (R/B) threshold method nowadays commonly adopted in most of the algorithms processing data from sky cameras and used to distinguish clear from cloudy sky pixels. Field images ~~, a red, a blue and a red and a blue trimmed with neural density were calibrated for the non-linearity of the basic sensor and for differences in the pass bands of the spectral filters and then~~ were used to obtain the corresponding blue to red ratio images before a threshold was set for determining the presence of thin clouds. It was found that uniform thin clouds gave rise to a significant increase in this ratio, lending themselves to detection. In a more recent version of the same algorithm (Shields et al., 2013) thin cloud detection is based on a haze/aerosol-corrected clear sky NIR/blue ratio image. The algorithm automatically corrects for aerosol/haze variations and hardware artefacts. Progress has been made over the years with the development of particularly promising algorithms for cirrus detection based on the use of polarizing filters (Horvath et al., 2002). Moreover it is speculated that cloud texture, the standard deviation of cloudy pixel brightness, lends itself to distinguishing light-textured cirrus from heavier-textured clouds such as cumuli (Long et al., 2006). However, the Red/Blue (R/B) threshold method and its improved version, the Red-Blue difference threshold technique, can fail in detecting cirrus (Heinle et al., 2010).

Nevertheless, sky imaging is effective for recording the optical displays sometimes associated with cirrus called halos and for measuring the angular distribution of scattered light. We will henceforth refer to this quantity Scattering Phase Function as the corrections applied to the measured radiance are intended to provide an approximation to the angular dependence of the unnormalized (1,1) element of the scattering matrix. From the scattering phase function (SPF) the halo ratio (HR) is then calculated, which has previously been proposed as the ratio of the intensity of light scattered at 22° to the one at 18.5°

(Auriol et al., 2001; Gayet et al., 2011), but was later obtained as the ratio of the average SPF between 21.5° and 22.5° to the average between 18.5° and 19.5° (Ulanowski et al., 2014), or as the ratio of the maximum of light scattered at an angle θ_{max} between 21° and 23.5° to the minimum of light scattered between 18° and θ_{max} (Forster et al., 2017). HR is a quantitative measure of the strength of the 22° halo ring, occurring when randomly oriented, hexagonal columns refract light through facets inclined at 60° to each other. In this respect modelling studies of SPFs (Macke et al., 1996; Baran and Labonnote, 2007; Um and McFarquhar, 2010; Liu et al., 2013) associate the presence of halos mostly with highly regular crystals, although some aggregates of smooth, regular prisms are also capable of producing halos (Ulanowski, 2005). Moreover, it has been shown on the basis of exact electromagnetic scattering techniques that the halo visibility implies the presence of large ice crystals with size parameter of the order of 100 or more (Mishchenko and Macke, 1998). Therefore the HR is an indirect measure of the size and regularity of the shape of the ice crystals forming the cloud. However, HR is also connected to cirrus reflectivity at solar wavelengths, in that the reflectivity is inversely proportional to the HR. This relates to other two important properties: ice crystal roughness and the asymmetry parameter *g*, the average cosine of the scattering angle (Macke et al., 1996). The former is expected to be negatively correlated with the HR as rough ice crystal SPFs show enhanced back and side scattering. Modelling studies have estimated that the global-averaged SW cloud radiative effect associated with this enhancement due to ice particle surface roughness is of the order of 1-2 W m^{-2} (Yi et al., 2013). In general roughening, internal inclusions and complex shapes are all major factors contributing to removing halo features from the SPFs (Shcherbakov, 2013). The asymmetry parameter on the other hand is expected to be positively correlated with the HR (Ulanowski et al., 2006; Gayet et al., 2011; Ulanowski et al., 2014). Many studies (Korolev et al., 2000; Garrett et al., 2001; Baran and Labonnote, 2006; Shcherbakov et al., 2006; Gayet et al., 2011; Baum et al., 2011; Cole et al., 2013; Ulanowski et al., 2014; Baran, 2015) suggest that cirrus clouds are mainly formed by rough or complex particles giving rise to typically featureless SPFs, confirming indications from previous observations and explaining the relative rarity of ground-observed halo occurrences (Sassen et al., 1994). Nevertheless, recent findings (Forster et al., 2017) suggest that the fraction of halo-producing cirrus might be larger than previously thought. This could be explained by modelling indicating that only a 10% fraction of smooth ice crystals is sufficient for the 22° halo display to occur. Less clear is the actual fraction of halo displays associated with preferentially oriented ice crystals. While Forster et al. (2017) observed more than 70% of total halo displays to be associated with oriented ice crystals, previous findings (Sassen et al., 2003) reported higher frequency of occurrence of 22° halos compared to sundogs and upper tangent arcs. To answer these questions further long term observations are needed, and we propose and implement for this purpose a technique based on retrieving the HR through all-sky imaging.

The details and specifications of the all-sky cameras used in this investigation are given in section 2.2, the camera calibration is covered in section 2.2.1, the testing and correcting of the lens projection is discussed in section 2.2.2, the method used for determining the ice cloud SPF from images is covered in paragraph 2.3. Corrections for vignetting and for air mass are described in sections 2.5 and 2.6, respectively. This is followed by detailed analysis of two test cases, where we also examine the issue of simultaneous detection of cirrus and its discrimination from warmer clouds.

2 Methods

2.1 Instrumentation

In addition to the all-sky cameras, the Cimel sun photometer CE318 N has been necessary to quantify image vignetting. The "Cimel" is a benchmark device for most aerosol observing networks and more specifically for the international federation of AERONET (Holben et al., 1998). Other observations, including brightness temperature (BT), measured through a narrow band infrared pyrometer (KT15.85 II, Heitronics) with spectral sensitivity peaking at about 10.6 µm, and solar irradiance, from pyranometer (SMP11, Kipp & Zonen B.V.) measurements have been used to confirm the presence of cirrus. The instrumentation was installed at the observatory at Bayfordbury (51.7748 N 0.0948 W) operated by the University of Hertfordshire.

2.2 The all-sky cameras

Two cameras were implemented, one set up for daytime, one for night-time observations. Both used the third version of the AllSky device, called the AllSky-340 (Santa Barbara Instrument Group, SBIG). Its optical system consists of a Kodak KAI-0340 CCD sensor and a Fujinon FE185C046HA-1 lens. The KAI-0340 is a VGA resolution (640x480 active pixels) 1/3" format CCD with 7.4 microns square pixels. The lens is of fish-eye type with a focal length of 1.4 mm and a focal ratio range of f/1.4 to f/16, fixed open at f/1.4 in the night camera and closed down to f/16 in the daytime camera. This combination gives a field of view of $185^\circ \times 144^\circ 47'$ and average resolution of $18'$ per pixel. Assuming the camera is aimed at the zenith, a maximum of 95.0% of the area of the sky can be imaged, with ~~2.52%~~ 2.5% cut off at the top and bottom. The areas around the edges are most affected by light pollution and not suitable for any measurements so this loss is not too detrimental. During this study the cameras were located on the roof of a two-storey building (about 8 m above ground) where the elevated vantage point from the roof gives a clear view of the skies, uninterrupted by most of the surrounding features such as trees. The cameras are connected to a computer via an RS-232 serial cable. Using a serial-USB adapter at the PC end the maximum download speed of ~~460.8 kbaud~~ 471.8 kbps can be achieved. At this rate the average download time of an image is 16.5 seconds for the gray camera. The colour one allows a download time of 48 seconds (Campbell, 2010).

The All-Sky cameras are illustrated in Fig. 1. Both cameras are inside aluminium enclosures with acrylic domes protecting the fisheye lens. A specially developed occulting disk was mounted on the daytime camera to prevent stray light from affecting the imaging. It consists of an opaque disk, 10 cm in diameter, connected to an L-shaped rigid arm whose long and short sections are 60 cm and 20 cm, respectively. The long arm is mounted on a stepper motor that can adjust its elevation angle, in turn attached to a ring which fits around the camera enclosure and can be rotated using a second stepper motor. Time, date and location provided by a GPS module (GPS-622R, RF Solutions) is fed to a microcontroller (PIC18F46K22) that calculates the sun's position (azimuth and elevation), when the sun is above the horizon. The controller operates the motors via two ST L6472 stepper motor drivers. At sunset the disk is positioned slightly below the horizon and microcontroller then waits for the sun to rise again.

The colour camera has a Bayer mosaic used for filtering the red, blue and green wavelengths. The Matlab built-in function "demosaic" is applied to the raw image data to reconstruct the full colour image. The fish-eye lens enables sky observation over a field of view (FOV) as large as 187°59′ along the ENE-WSW direction and as large as 142°38′ along SSE-NNW. The FOV of the daytime camera along ENE-WSW is slightly larger, 189°53′. The difference is due to the different alignment of the lens relative to the sensor. This is also reflected in the position of the true zenith (x_0, y_0) with respect to the centre of the camera plane, which for both cameras does not coincide with the true zenith. An offset of 14 pixels in the x direction and 12 pixels in the y direction that corresponds to about 4° and 3.5° respectively has been measured for the night time camera and about 1° and 9.5° for the daytime camera. The fish-eye lens employed in both cameras uses the "f-theta", or equidistant projection system which means that the distance in pixels from the true zenith of the object projected onto the camera plane is simply a scaling factor f (here 3.365 pixels/degree) multiplied by the zenith angle z of the object expressed in degrees (see section 2.2.1). The output images are available either in JPG or FITS format but the latter is preferred because of larger dynamic range and the absence of "digital development" correction.

2.2.1 Camera calibration

Geometric calibration of the camera is done by detecting the position of specific stars and planets in a night-time image and implementing a minimization procedure. This was achieved by using four images, taken at different times of night so that bright stars were available in all quadrants of the image. Over the course of a clear night the daytime camera, whose aperture had been increased from the usual f/16 to f/1.4, was left to take images. Bright stars trajectories were plotted as curves on an image, based on their position in the middle of the exposure, the predicted movement and the theoretical f-theta system of the lens. The projection parameters of the camera were then adjusted until the errors between the calculated and true position of the stars on the image were minimized. The procedure will now be described in detail. First, the time the current image was taken was converted to the Julian date. Knowing this time and the longitude and latitude of the camera, the altitude and azimuth of the stars could be calculated from their right ascension and declinations (Meeus, 1998). These coordinates were transformed into the 2D plane of the image using the f-theta system, found to provide a good initial fit, then were shifted and rotated to account for the fact that the camera does not actually point precisely at the zenith, nor is the image top perfectly aligned with the true north. Finally ~~the~~ an empirical scaling factor was applied to the coordinates in the x and y direction ~~to compensate for the distortion created by the lens. This was found by plotting stars using the preliminary projection and determining the difference between the plotted stars and their corresponding background star. The errors as a function of the x, and then y directions were fitted to a bi-cubic function and these added to the coordinates.~~ With the preliminary f-theta model so modified the camera parameters were manually adjusted until the difference between the plotted stars and their corresponding background star was minimized. The final result was found to align well to the background stars in the central parts of the image, and slightly less well around the edges. The equations which map astronomic coordinates into camera ones are:

$$x = f z \sin(A - \Delta) + x_0 \tag{1}$$

$$y = f z \cos(A - \Delta) + y_0 \tag{2}$$

where (z , A) are the zenith and azimuth angles, Δ is the rotation of the camera from north, measuring about 16.4° and 13.6° for the night and day time cameras, respectively, (x_0,y_0) are the pixel coordinates of the actual zenith and f is the scale factor. The latter was found to be 3.365 px/deg. If d is the pixel distance from zenith then the above equations can be rewritten as:

$$d = f z = \sqrt{(x - x_0)^2 + (y - y_0)^2} \tag{3}$$

2.2.2 Testing of the lens projection

In order to test the reliability of Eq. (1) and (2) in reproducing the actual mapping of the lens the same equations were used to track star and planet trajectories. On a clear night an image was acquired. Given A, z and the acquisition time, pixel coordinates (x, y) of a celestial object can be determined through Eq. (1) and (2). The actual location is detected by locating the bright spot that corresponds to the star/planet. This is done by selecting an appropriate brightness threshold and converting the image to binary. From the binary image a square region centred where the star/planet is predicted to be (x, y), and sufficiently large to include the spot, is then selected. The centre of mass of the spot then becomes the actual position. Fig. 2 shows predicted (blue dots) and actual positions (red dots) of several celestial objects on the night of the 15th of February 2013. The mean difference between predicted and actual position was mostly <0.1° aside from portions of Vega's, Deneb's, Arcturus', Sirius' and Rigel's trajectories for which larger discrepancies, up to 0.38°, were observed. These relatively larger deviations are associated with the decreased accuracy of the method due to light pollution especially significant as the horizon is approached. For these reasons the lens projection was judged to be reasonably well replicated by the Eq. (1) and (2). Consequently, the following image transformations were implemented using exclusively the f-theta system.

2.3 Geometric transformations

The SPF is obtained by averaging the image brightness over pixels which are equidistant from the light source in terms of scattering angle. To achieve this, the raw image is transformed to move the light source to the zenith, to give a light-source centred system of coordinates. This is accomplished by mapping the original coordinates onto a sphere of unit radius and then by rotating the spherical coordinates to centre the light source at the origin of the final system. The first step consists in changing the projection from "linear" with respect to z to proportional to sin z. Given d, from Eq. (4) z is determined for each pixel (x, y) and the new coordinates (x', y') are calculated. The change of projection can be seen as the wrapping of the raw image around a sphere of unit radius with the constraint that the horizon, in the new coordinate system, will now be at a unit distance from the zenith. The periphery of the image which is below the horizon (see Fig. 3) is projected in the lower hemisphere while points above the horizon appear in the upper hemisphere.The projection of the raw image of Fig. 3 in the upper hemisphere is shown in Fig. 4. The new coordinates x' and y' determine the Z coordinate: pixels above and below the horizon are associated with

positive and negative Z, respectively. A rotation transformation $\mathbf{T}$ is then used to rotate the coordinates (x′, y′, Z) of a generic pixel, identified by the vector $\boldsymbol{P}$, around the unit vector u that is perpendicular to the line linking the true zenith and the light source, by an angle θ equal to the light source zenith angle (see Fig. 4) according to:

$$\mathbf{T}(\boldsymbol{P}) = (1 - \cos\theta)(\boldsymbol{P} \cdot \hat{u})\hat{u} + \cos\theta\boldsymbol{P} + \sin\theta(\boldsymbol{P} \times \hat{u}) \tag{4}$$

With the rotated coordinates (x", y", Z′) available, the transformed image in the upper hemisphere can be obtained, and an example is shown in Fig. 5. This can be achieved by interpolating the original image into the new coordinates. Pixels that belong to those portions of the image that after rotation would be below the new horizon are in the lower hemisphere, which is not shown here. This should be accounted for if the SPF is to be calculated for all aky pixels and scattering angles available. Nevertheless that portion of the SPF is not necessary for HR calculation purposes and will not be covered here. The interpolated image is ultimately used to calculate the brightness as a function of the scattering angle by averaging over the entire azimuth angle range. Fig. 6 (red-dashed line) shows the end result corresponding to the raw image from Fig. 3.

2.4 Background mask

To prevent the contamination of the sky image by background objects above the horizon, a mask, derived from a summer time image, when vegetation is thicker, was used. To prevent the mask edge from falling within the region of the SPF (between 18° and 22°) from which the HR is derived, the measure was limited to images such that the light source $z < 65°$.

2.5 Vignetting correction

The falloff of brightness for increasing z, associated with vignetting, takes place in nearly every digital photograph, in all optical lens systems, in particular wide-angle and ultra wide-angle lenses like fisheye lenses (Jacobs and Wilson, 2007). Optical and natural vignetting are associated with smaller lens opening for obliquely incident light and the $\cos^4$ law of illumination falloff, respectively, both inherent to any lens design (Ray, 2002). In general, vignetting increases with the aperture and decreases with the focal length. Here it is quantified by comparing daytime image data with sun photometer data under clear sky. While the camera is affected by vignetting, the sun photometer is not, hence the ratio of the corresponding radiance measures, over a similar spectral range, can be used to quantify vignetting. The blue channel of a clear sky daytime RGB image was extracted, being the best match to a spectral channel of the sun photometer and having larger quantum efficiency and narrower spectral width of the response than the green and red channels. ~~The image brightness along the principal plane (containing the zenith and the sun) and the corresponding sun photometer output were compared~~ The sun-photometer measurement along the solar principal plane, performed every hour, over the various wavelengths, one at a time, about 35 s apart, were compared to the corresponding image brightness from the closest camera measurement; ~~by neglecting~~ As vignetting is assumed to be symmetric under rotations around the camera zenith, pixels such that z is greater than approximately 20° over the meridian containing the sun~~,~~ were neglected and the average of the sun photometer sky brightness at the visible wavelengths of 0.5015 µm and 0.4403 µm was LOWESS (*Locally Weighted Scatterplot Smoothing*) smoothed and fitted. Analogously a polynomial was fitted to the

LOWESS smoothed image data. The ratio between the two fitting polynomials (camera to sun photometer) after normalization (see Fig. 7) is what we refer to as the devignetting coefficient (DC, see Fig. 8 black curve). As the DC was expected to be monotonically decreasing with z, ~~the presence of a peak located roughly 8° from the zenith~~ the shift of the maximum from the zenith to the position at roughly 8° was investigated. Since the use of the occulting disk allows us to exclude stray light is the cause of it, the simplest explanation comes from observing that such an off-set, corresponding to around 27 pixels, corresponds to a displacement of only 0.2 mm between the lens axis and the centre of the aperture. To form a correction function symmetric about the zenith, the original curve was "mirrored" about the zenith (see Fig. 8, red curve), then a Gaussian of the form shown in Eq. (5) was fitted to the average of the original and the mirror curve (see Fig. 8, dashed curve).

$$f(z) = A + B \cdot \mathrm{e}^{-(z/C)^2} \tag{5}$$

A, B and C so obtained are 0.74, 0.26 and 40.03, respectively. The fitting curve provides a working approximation of the actual DC. Fig. 6 (black-dashed line) shows the SPF corresponding to the raw image from Fig. 3 when geometric, AM, vignetting and mask corrections are included. The latter removes the contamination associated with objects in the field of view, such as trees.

The vignetting correction so obtained is intended to be generic. Since the correction is nearly rotationally symmetric, and we have concluded that the residual asymmetry is the outcome of a small misalignment of the sensor, which is likely to vary between cameras, the generic, symmetric correction can be applied to sites where deriving a camera-specific correction is not possible due to the absence of a sun photometer.

2.6 Air mass correction

The additional scattering that light undergoes for slant paths is associated with increased image brightness, evident for large z. In this context we will be assuming single scattering approximation. To model relative air mass (AM), the ratio of the absolute optical air mass M calculated along z to the zenith air mass M_0, a non-refracting homogeneous radially symmetric atmosphere was assumed. This provides realistic values of AM near the horizon, where it is less than 40 as it is expected (Rapp-Arraras and Domingo-Santos, 2011). Each pixel brightness was then corrected by dividing ~~for~~ by the corresponding AM(z). With this correction in place averaging of sky brightness along lines of constant scattering angle becomes possible. However, a kink in the SPF, at a scattering angle corresponding approximately to the edge of the mask, was observed. This is ascribable to the large value that the AM takes for large z, causing the image brightness to drop rapidly. If such values of the AM are excluded from the correction the kink gets significantly reduced. Furthermore for large solar z a cut-off angle that is too large can cause the HR to decrease due to multiple scattering affecting the part of the halo below the sun. It has been shown previously through radiative transfer calculations accounting for multiple scattering that the brightness of the lower part of the halo reaches a maximum for smaller cloud optical thickness τ than the portion above the sun (Gedzelman and Vollmer, 2008). By setting the cut-off at z=70° the SPF becomes smooth and multiple scattering effects are reduced, while avoiding seasonal bias due to the solar z range covered during the year.

2.7 Cirrus discrimination

A quantification of the temporal fluctuations of the infrared brightness temperature BT is expressed in terms of the fluctuation coefficient FC. The FC is obtained here through Detrended Fluctuation Analysis (DFA) of the BT, and is expressed as the exponent of the DFA function ~~expressed as~~ following a simple power law (Brocard et al., 2011). It allows detecting the presence of clouds, unless very thin optically. In fact BT fluctuates significantly under optically thick clouds while under clear sky it follows the relatively slow-changing water vapour diurnal cycle. Therefore clear sky FC allows setting a threshold (DFA threshold) for the transition from clear to cloudy sky. This threshold was ~~found~~ chosen empirically to be 0.02 on the basis of the DFA output calculated ~~every 20 minutes and over a time scale ranging between 60 and 150 seconds~~, unlike in Brocard et al. (2011), every 5 minutes, over data sampled with 1 s resolution and for time intervals ranging between 20 and 60 seconds. The intervals were chosen as the time range over which the DFA function was relatively stable and the slope of the function (the FC) was as sensitive as possible to the presence of clouds. The DFA algorithm was applied to one year of data and the corresponding FC time series was averaged over clear sky periods to set the DFA threshold. This was obtained after manual cloud screening of images associated with minima of the fluctuation coefficient. Furthermore, we wish to point out that like in Brocard et al. (2011) the initial analysis step of cumulative summation (integration) of the time series was not carried out. We note that cumulative summation of a self-affine series shifts the FC by +1 (Heneghan and McDarby, 2000), so the threshold applied here would have a value close to 1 if a standard DFA procedure was followed. Separately, a departure from modelled clear sky BT due to the presence of relatively optically thick cirrus can provide a BT threshold (Ci threshold) that was used for assessing cloud phase. A simple analytical model of downwelling thermal radiation under clear skies was implemented for this purpose. The model uses ground-level air temperature and integrated water vapour path (retrieved locally from GNSS delays) as input parameters to estimate clear sky BT at the central wavelength of the pyrometer (Dandini, 2016). In order to establish via BT whether warm or cold clouds are present in the field of view of our instrument, an estimate of the departure of BT from clear sky BT due to cirrus was calculated. We set the maximum possible departure from clear sky BT attributable to cirrus as the one when the cloud is warmest and optically thick. Warm liquid clouds would certainly determine a departure from clear sky BT larger than the one due to such cirrus and hence would lend themselves to be discriminated. By assuming an optically thick cirrus (emissivity of 1) at a temperature of -38°C, representative of the upper temperature limit of ice clouds (Heymsfield et al., 2017), an estimate of the irradiance due to the direct emission of cirrus corrected for the atmospheric attenuation and emission~~,~~ was obtained, and converted to brightness temperature by inverting Planck's law (see Fig. 10 and 12, middle plot, black dashed line). The Ci threshold follows the diurnal water vapour cycle corrected for the attenuated contribution of such thick cirrus. Above this threshold we can expect optically thick clouds warmer than -38°C, i.e. theoretically not cirrus. Hence, HR time series corresponding to two test cases discussed in the coming section are complemented by simultaneous comparisons of BT, with the Ci threshold, and the FC with the DFA threshold, as well as broadband downwelling irradiance I.

3 Results and discussion

We now contrast two case studies based on two consecutive days of observations. Halo ratio time series were obtained on the 6th of July 2016 between 8 and 11 am, when halo and non-halo cirrus alternated with scattered cumuli- see Fig. 9 and on the 7th of July 2016 between 12 noon and 3 pm, when mostly cirrus occurred - see Fig. 11. All-sky images corresponding to HR minima and maxima are shown as inserts in the figures. Arrows, specifying the time the image was acquired, are black if the halo is either absent or faint, and yellow otherwise. In variance from the previous definitions of the HR (see Introduction), it was determined as the ratio of the SPF at slightly larger angles: 23° and 20°, which correspond to the locations of the maximum and minimum we typically found in the measured SPF, respectively. This finding corroborates that of Lynch et al. (1985) who observed these values to be 22.8° and 19.7°, respectively. This change resulted in enhanced sensitivity of the HR to the halo status of cirrus - see Fig. 10 and Fig. 12, top plots. The shift of the halo peak towards larger angles than the 22° shown by the more familiar single-scattering SPF computed from geometric optics can be interpreted as originating from the combined contributions from background sky scattering, diffraction effects (due to small crystal size) and crystal roughness (Macke et al., 1996; Ulanowski et al. 2005; Liu et al., 2013; Smith et al., 2015).

3.1 Test case 1: 6th of July 2016

On the 6th of July between 8 and 10 am cirrus occurs as all-sky camera, BT observations and FC measures all show - see Fig. 10. The FC is nearly always above the DFA threshold while the BT is below the Ci threshold. Over this time window, on qualitative grounds, the behaviour of the BT and the solar irradiance suggests that the HR increases with the optical thickness τ (see Fig. 10, middle and bottom plots). This is consistent with the results of simulations (Khokanowsky, 2008), based on ray tracing techniques incorporating physical optics (Mishchenko and Macke, 1998) and neglecting molecular and aerosol scattering, that show a linear increase of halo contrast with increasing τ up to τ=3 and a decrease for τ>3 due to multiple scattering. Between about 8 and 8:20 am the HR, mostly <1, shows a maximum and a minimum at about 8:06 and 8:12 am, respectively, when a relatively faint 22° halo is visible. Maxima with HR>1, on the other hand, are measured at 8:33 and 9:06 am, when bright-halo is observed, and at 9:30 am when lower halo brightness is associated with decreased HR. Similarly, the attenuated halo brightness at about 8:51 am corresponds to an HR minimum. Between 9:36 and 10 am the HR drops below 1 and cirrus gets thinner. The small local maxima observed over the same time window at about 9:38, 9:45 and 9:54 am are ascribable to cirrus optical depth variations. From 10 am, as cirrus disperse, cumuli start entering the field of view of the camera. A local HR maximum is then measured at 10:03 am whereas HR values >1 at 10:16, 10:33 and 11 am, while scattered cumuli over a mostly clear background increasingly occur. The FC testifies to the presence of clouds whereas the BT becomes larger than the Ci threshold only at about 10:54 am, probably because of the sparse nature of the cumuli preventing significant direct radiation from falling within the field of view of the radiometer. However, dips of the solar irradiance I at approximately 10:24, 10:32 and 10:42 am, indicating increased optical depth, are also observed. While on an overcast day global irradiance depends primarily on diffuse irradiance (Kaskaoutis et al., 2008), on a partly cloudy day clouds crossing the sun path are the main factor to determine variations in the signal of the pyranometer. In particular the ratio of diffuse to global

irradiance has been estimated to be 0.15, 1 and > 0.15 under clear, overcast and partly cloudy sky, respectively (Duchon and O'Malley, 1999; Orsini et al., 2002). These relatively large HR values are artefacts caused by the image becoming brighter at larger scattering angles, possibly due to bright cloud edges. Such cases should be screened out from the analysis as the HR parameter applies to ice clouds only. This example shows that while a relatively large HR (HR>1) can be an indication of the presence of halo-producing cirrus, this does not have always to be the case.

3.2 Test case 2: 7th of July 2016

On the 7th of July between 12 noon and 3 pm the sky is mainly characterized by the presence of cirrus, except between about 12 and 12:30 pm when sparse cumuli are seen, around 12:45 pm when relatively opaque altocumuli occur, between around 1:30 and 1:48 pm and about 2:15 pm when cumuli overlap with the cirrus background - see Fig. 11. Correspondingly, the FC is always above the DFA threshold, while the BT is mostly below the Ci threshold although larger values are observed at about 12:20, 12:27, 12:42, 12:48, 1:40, 2:15 and 2:18 pm when, as expected, the solar irradiance I drops. The HR peaks measured at about 12:06 and 12:18 pm, in similarity with the previous case, appear to be associated with bright cloud edges. Between 12:30 and 12:38 pm, when bright-halo is visible, the HR is >1 and then decreases until about 12:42 pm by which time the halo is no longer visible, possibly due to multiple scattering associated with the increased τ, as demonstrated by decreased solar irradiance at that point - Fig. 11. With halo producing cirrus present again from 12:50 pm, the HR increases, except for a local minimum at about 1 pm, until about 1:18 pm, when it becomes larger than 1 and the halo is correspondingly sharper. The HR then drops fairly steadily, except for a local maximum at about 1:30 pm, while the halo, still partly visible, fades gradually away to eventually disappear by about 1:36 pm. This is when, we hypothesize, cloud τ has become <1 and Rayleigh and aerosol scattering contribute to the halo contrast reduction. A faint halo present from about 1:45 pm gets quite sharp by 2 pm as the HR becomes again larger than 1. The halo brightness then stays constant for about ten minutes before the HR reaches another minimum at about 2:12 pm, when cumuli are seen by the camera. As the halo sharpness increases, the HR also increases fairly uniformly until about 2:28 pm, when a maximum of 1.14 is reached. We speculate, based on previous findings (Forster et al., 2017; Khokanowsky, 2008), that this is when τ, probably somewhere between 1 and 3, becomes significantly larger than Rayleigh and aerosol optical thickness without exceeding the optical depth beyond which multiple scattering becomes dominant. The HR then drops to 1 in less than 20 minutes, while the halo is still fairly bright, and continues to go down until 3 pm when the halo is eventually no longer visible. Peaks at about 2:40 and 2:54 pm are due to rapid variations in sky brightness, associated with cumuli like those observed at near 2:38 pm, which, in analogy with the minima seen at 2:12 and 1:48 pm, cause the SPF to vary significantly as the cumuli transit over the cirrus. With an average BT roughly 10°C higher than on the previous day, this is a case of relatively warm halo-producing cloud, yet the relatively large HR indicates that the cloud is dominated by ice.

Overall the HR correlates well with the fluctuating halo visibility observed throughout the periods examined. According to previous radiative transfer calculations (Forster et al., 2017), we conjecture that in order to observe the absolute HR maxima

measured for the two cases discussed here a certain minimum fraction of smooth hexagonal ice columns had to be present. ~~If multiple scattering were to be accounted for, such a fraction could be an underestimation of the actual one.~~

4 Conclusions

A method for the retrieval of the halo ratio HR from all-sky imaging has been proposed. This consists of applying a series of image transformations and corrections needed to interpret images quantitatively in terms of the scattering phase function. Halo formation can then be identified by taking a ratio of phase function values at particular scattering angles in the vicinity of the halo peak. Unlike in previous studies which tended to use slightly smaller angles (Auriol et al., 2001; Gayet et al., 2011; Ulanowski et al., 2014; Forster et al., 2017) we have used a ratio at scattering angles of 23° and 20° corresponding to the locations of the maximum and minimum we typically found in the measured SPF, respectively. The new angles result in higher values of the HR from our data than the HR definitions cited above. After applying the corrections and transformations, HR time series have been shown for two test cases, the 6^{th} and 7^{th} of July 2016. HR values ≥ 1 were observed under halo producing cirrus, but also sometimes under scattered low-level clouds when HR maxima appeared to be artefacts due to bright cloud edges. As previously predicted (Kokhanovsky, 2008) multiple scattering appears to lead to decreased HR. We have partly counteracted this by excluding from the HR calculations pixels at z>70°. However, in future it would be possible to exclude the lower parts of the halo where the slant optical thickness is too large. This implies having to estimate the cirrus optical thickness τ, which could be derived from pyranometer measurements, for example (Fitzpatrick et al., 2005; Qiu, 2006) - allowing, by the way, to verify the expected relation between HR and τ which sets a maximum HR at τ=1 (Forster et al., 2017). Overall the HR is shown to be sensitive to the halo status of cirrus as it is well correlated with halo visibility. All-sky cameras have the advantage of being relatively cheap when compared to more complex and difficult to align tracking systems such as the HaloCam (Forster et al., 2017). Moreover like the sun-tracking camera used by Foster et al. (2017), who have quantified the shift of the red tinged inner edge of the 22° halo, colour all-sky cameras can also provide spectral dependence.

However, the all-sky camera data should also be supplemented with additional information if the HR observations are to be associated only with cirrus: a separate cirrus detection method is necessary to screen out non-ice clouds and clear sky periods, before deriving reliable HR statistics. The quantification of the fluctuations of the brightness temperature BT, expressed in terms of the fluctuation coefficient FC, has been used to discriminate clouds from clear sky by comparing the FC to the DFA threshold which is used to set the transition from clear to cloudy skies. However, for very small τ the fluctuations of the BT can be of similar magnitude as under clear sky, putting a limit on this technique in the context of very thin cirrus. Additionally, an estimate of the magnitude of the BT in the presence of optically thick cirrus has been used as an indicator of cloud phase. This method has managed to detect cirrus most of the time over the periods of observation. However it was unable to discriminate some of the scattered cumuli, sometimes associated with high HR values that have to be screened out from the analysis, and in one case failed to confirm the presence of ice, as shown by the presence of the 22° halo. Where no other sky observations are available and attenuation of solar irradiance due to aerosol can be measured or accounted for, a method previously implemented for solar irradiance time series from pyranometer measurements can be used for cloud classification

(Duchon and O'Malley, 1999). This can be achieved by accounting for the standard deviation of the scaled observed irradiance and the ratio of the former to the scaled clear sky irradiance (Duchon and O'Malley, 1999) or, as a cheap and relatively easy to use alternative, by combining observed total irradiance, temperature and relative humidity (Pagès et al., 2003). In the future these cirrus discrimination methods should be compared to techniques such as microwave radiometry or lidar which would allow us to assess their relative merit. As an alternative to BT radiometry the backscattered signal from lidar can be used to discriminate between cloudy and clear skies. If depolarization information is not available cloud phase discrimination can be achieved from cloud base height by estimating cloud base temperature. Such estimates can be improved if temperature profiles are available from radiosonde ascents (Forster et al., 2017). While this brings the advantage that the cloud base temperature will be less sensitive to τ than the temperature from the radiometer on the other hand this method requires additional measurements. However it can be considered an alternative if such measurements are available at the given observation site.

Ultimately, the method proposed here is meant to provide cirrus characterization. The two test cases analysed show the presence of large (compared to wavelength, probably characterized by size parameters larger than 100 - Mishchenko and Macke, 1998) and regular, smooth ice crystals. Results of previous investigations (Forster et al., 2017) have been used to speculate on such smooth crystal fraction. We argue that when the 22° halo was visible a percentage of at least 20% of regular ice crystals had to be present ~~if molecular, aerosol and multiple scattering in addition to surface albedo are accounted for, together contributing to a reduction of the halo contrast~~. We have also conjectured that when the HR reached its absolute maxima the fraction of such pristine crystals is likely to have been much larger than 20%. The remaining fraction could have been composed of irregularly shaped, complex, rough or small ice crystals.

Long term observations of halo displays, preferably at multiple sites, must be carried out to allow obtaining statistics of the occurrence of halo producing cirrus, which still remains unknown. The magnitude of the HR could then be used to assess aspects of the composition of the cirrus - while remembering that low HR can have multiple causes, as discussed above. Furthermore, by extending the method to additional halo displays further information on ice crystal geometry could potentially be obtained - e.g. the presence of sun dogs and the 46° halo indicates the presence of aligned plates and solid columns, respectively.

The utilisation of the all-sky cameras to transform the measured light intensity into the scattering phase function and, on a limited extent, the cirrus detection algorithm, are the particularly novel aspects of this work; this has not been done previously to the best of our knowledge. The method applied to the all-sky images in particular, allowing the measurement of the distribution of sky radiance, permits taking advantage of the large field of view associated with the all-sky imaging in a quantitative manner. Consequently, while not computationally demanding and relatively easy to implement, this method allows broadening the range of application of the all-sky imaging beyond the more qualitative recording of cloud fields and optical displays associated with cirrus. The cloud classification method, on the other hand, is original in that relies on a non-fixed, non-location specific and easy to model temperature threshold. The combined use of these two methods, allows relatively inexpensive halo observations and the retrieval of information pertaining to ice particles size and texture. If implemented at multiple locations, the methods can provide a useful dataset for improving the understanding of cirrus composition.

Competing interests. No competing interests are present.

Acknowledgements. The services of the Natural Environment Research Council (NERC) British Isles continuous GNSS Facility (BIGF), www.bigf.ac.uk, in providing archived GNSS products to this study, are gratefully acknowledged. We thank Prof. Paul Kaye for his contribution to designing the occulting disc, Dr. Evelyn Hesse (University of Hertfordshire) and Dr. Anthony Baran (Met Office) for their valuable advice. Z. Ulanowski acknowledges support from the Natural Environment Research Council grant NE/I020067/1.

References

Allmen, M., and Kegelmeyer Jr., W. P.: The computation of cloud-base height from paired whole-sky imaging cameras, J. Atmos. Ocean. Tech., 13, 97-113, doi:10.1175/1520-0426(1996)013<0097:TCOCBH>2.0.CO;2, 1996.

Auriol, F., Gayet, J. F., Febvre, G., Jourdan, O., Labonnote, L., and Brogniez, G.: In situ observations of cirrus cloud scattering phase function with 22° and 46° halos: cloud field study on 19 February 1998, J. Atmos. Sci., 58, 3376-3390, doi:10.1175/1520-0469(2001)058<3376:ISOOCS>2.0.CO;2, 2001.

Baran, A. J., and Labonnote, L. C.: A self consistent scattering model for cirrus, I: the solar region, Q. J. Roy. Meteor. Soc., 133, 1899-1912, doi:10.1002/qj.164, 2007.

Baran, A. J.: From the single-scattering properties of ice crystals to climate prediction: A way forward, J. Atmos. Res., 112, 45-69, doi:10.1016/j.atmosres.2012.04.010, 2012.

Baran, A. J., Furtado, K., Labonnote, L. C., Havemann, S., Thelen, J. C., and Marenco, F.: On the relationship between the scattering phase function of cirrus and the atmospheric state, Atmos. Chem. Phys., 15, 1105-1127, doi:10.5194/acp-15-1105-2015, 2015.

Baum, B. A., Yang, P., Heymsfield, A. J., Schmitt, C., Xie, Y., Bansemer, A., Hu, Y. X., and Zhang, Z.: Improvements in short-wave bulk scattering and absorption models for the remote sensing of ice clouds, J. Appl. Meteor. Climatol., 50, 1037-1056, doi:10.1175/2010JAMC2608.1, 2011.

Berger, L., Besnard, T., Genkova, I., Gillotay, D., Long, C.N., Zanghi, F., Deslondes, J.P., and Perdereau, G.: Image comparison from two cloud cover sensor in infrared and visible spectral regions, in: Proceedings of the 21st International Conference on Interactive Information Processing Systems (IIPS) for Meteorology, Oceanography, and Hydrology, San Diego - CA, 9-13 January, 2005.

Brocard, E., Schneebeli, M., and Mätzler, C.: Detection of cirrus clouds using infrared radiometry, IEEE T. Geosci. Remote, 49, 595-602, doi:10.1109/TGRS.2010.2063033, 2011.

Calbó, J., and Sabburg, J.: Feature extraction from whole-sky groundbased images for cloud-type recognition, J. Atmos. Ocean. Tech, 25, 3-14, doi:10.1175/2007JTECHA959.1, 2008.

Calbó, J., Page‘s, D., and González, J.A.: Empirical studies of cloud effects on UV radiation: a review, Rev. Geophys., 43, 1-28, doi:10.1029/2004RG000155, 2008.

Campbell, D.: Widefield Imaging at Bayfordbury Observatory, B. S. thesis, University of Hertfordshire, Hatfield, 47, 2010.

Cazorla, A., Olmo, F.J., and Alados-Arboledas, L.: Using a sky imager for aerosol characterization, Atmos. Environ., 42, 2739-2745, doi:10.1016/j.atmosenv.2007.06.016, 2008a.

Cazorla, A., Olmo, F.J., and Alados-Arboledas, L.: Development of a sky imager for cloud cover assessment, J. Opt. Soc. Am., 25, 29-39, doi:10.1364/JOSAA.25.000029, 2008b.

Chow, C.W., Urquhart, B., Dominguez, A., Kleissl, J., Shields, J., and Washom, B.: Intra-hour forecasting with a total sky imager at the UC San Diego solar energy testbed, Sol. Energy, 85, 2881-2893, doi:10.1016/j.solener.2011.08.025, 2011.

Cole, B. H., Yang, P., Baum, B. A., Riedi, J., Labonnote, L. C., Thieuleux, F., and Platnick, S.: Comparison of PARASOL observations with polarized reflectances simulated using different ice habit mixtures, J. Appl. Meteorol. Clim., 52, 186-196, doi:10.1175/JAMC-D-12-097.1, 2013.

Dandini, P.: Cirrus occurrence and properties determined from ground-based remote sensing, PhD, University of Hertfordshire, Hatfield (UK), 213, 2016.

Duchon, C.E., and O'Malley, M.S.: Estimating cloud type from pyranometer observations, J. App. Meteorol., 38, 132-141, doi:10.1175/1520-0450(1999)038<0132:ECTFPO>2.0.CO;2, 1999.

Fitzpatrick, M.F. and Warren, S.G.: Transmission of solar radiation by clouds over snow and ice surfaces. Part II: Cloud optical depth and shortwave radiative forcing from pyranometer measurements in the Southern Ocean, J. Climate, 18, 4637-4648, doi:10.1175/JCLI3562.1, 2005.

Forster, L., Seefeldner, M., Wiegner, M., and Mayer, B.: Ice Crystal Characterization in Cirrus Clouds: A Sun-tracking Camera System and Automated Detection Algorithm for Halo Displays, Atmos. Meas. Tech., 10, 2499-2516, doi:10.5194/amt-10-2499-2017, 2017.

Garrett, T. J., Hobbs, P. V., and Gerber, H.: Shortwave, single scattering properties of arctic ice clouds, J. Geophys. Res., 106, doi:15155-15172, 10.1029/2000JD900195, 2001.

Gayet, J. F., Mioche, G., Shcherbakov, V., Gourbeyre, C., Busen, R., and Minikin, A.: Optical properties of pristine ice crystals in mid-latitude cirrus clouds: a case study during CIRCLE-2 experiment, Atmos. Chem. Phys., 11, 2537-2544, doi:10.5194/acp-11-2537-2011, 2011.

Gedzelman, S. D., and Vollmer, M.: Atmospheric optical phenomena and radiative transfer, B. Am. Meteorol. Soc., 89, 471-485, doi:10.1175/BAMS-89-4-471, 2008.

Ghonima, M. S., Urquhart, B., Chow, C. W., Shields, J. E., Cazorla, A., and Kleissl, J.: A method for cloud detection and opacity classification based on ground based sky imagery, Atmos. Meas. Tech., 5, 2881-2892, doi:10.5194/amt-5-2881-2012, 2012.

Heinle, A., Macke, A., and Srivastav, A.: Automatic cloud classification of whole sky images, Atmos. Meas. Tech., 3, 557-567, doi:10.5194/amt-3-557-2010, 2010.

Heneghan, C., and McDarby, G.: Establishing the relation between detrended fluctuation analysis and power spectral density analysis for stochastic processes, Phys. Rev. E 62, 6103-6110, doi:10.1103/PhysRevE.62.6103, 2000.

Heymsfield, A., Kramer, M., Brown, P., Cziczo, D., Franklin, C., Lawson, P., Lohmann, U., Luebke, A., McFarquhar, G. M., Ulanowski, Z.: Cirrus clouds, Meteor. Monographs, 58, 2.1-2.26, doi:10.1175/AMSMONOGRAPHS-D-16-0010.1, 2017.

Holben, B., Eck, T., Slutsker, I., Tanré, D., Buis, J., Setzer, A., Vermote, E., Reagan, J., Kaufman, Y., Nakajima, T., Lavenu, F., Jankowiak, I., and Smirnov, A.: AERONET - A Federated Instrument Network and Data Archive for Aerosol Characterization, Remote Sens. Environ., 66, 1-16, doi:10.1016/S0034-4257(98)00031-5, 1998.

Horvath, G., Barta, A., Gal, J., Suhai, B., and Haiman, O.: Ground-based full-sky imaging polarimetry of rapidly changing skies and its use for polarimetric cloud detection, Appl. Optics, 41, 543-559, doi:10.1364/AO.41.000543, 2002.

Jacobs, A., and Wilson, M.: Determining lens vignetting with HDR techniques, XII National Conference on Lighting, Varna, Bulgaria, 10-12 June 2007, 2007.

Janeiro, F.M., Ramos, P.M., Wagner, F., and Silva, A.M.: Developments of low-cost procedure to estimate cloud base height based on a digital camera, Measurements, 43, 684-689, doi:10.1016/j.measurement.2010.01.007, 2010.

Johnson, R. W. and Hering, W. S.: Automated cloud cover measurements with a solid state imaging system, Tech. note 206, Visibility Laboratory, University of California, San Diego, Scripps Institution of Oceanography, La Jolla, CA, 11 pp., 1987.

Kassianov, E. I., Long, C. and Ovtchinnikov, M.: Cloud sky cover versus cloud fraction: Whole-sky simulations and observations, J. Appl. Meteor., 44, 86-98, doi:10.1175/JAM-2184.1, 2005.

Kaskaoutis, D.G., Kambezidis, H.D., Kharol, S.K., and Badarinath, K.V.S.: The diffuse-to-global spectral irradiance ratio as a cloud-screening technique for radiometric data, J. Atmos. Sol-Terr. Phy., 70, 1597-1606, doi:10.1016/j.jastp.2008.04.013, 2008.

Kegelmeyer, W. P.: Extraction of Cloud Statistics from Whole Sky Imaging Cameras, SANDIA Report, SAND94-8222, Sandia National Laboratories Albuquerque, New Mexico and Livermore, CA, 17 pp., 1994.

Kokhanovsky, A.: The contrast and brightness of halos in crystalline clouds, Atmos. Res., 89, 110-112, doi:10.1016/j.atmosres.2007.12.006, 2008.

Korolev, A., Isaac, G. A., and Hallett, J.: Ice particle habits in stratiform clouds, Q. J. Roy. Meteor. Soc., 126, 2873-2902, doi:10.1002/qj.49712656913, 2000.

Liu, C., Panetta, R. L., and Yang, P.: The effects of surface roughness on the scattering properties of hexagonal columns with sizes from the Rayleigh to the geometric optics regimes, J. Quantit. Spectr. Ra., 129, 169-185, doi:101016/jjqsrt201306011, 2013.

Long, C. N.: Correcting for circumsolar and near-horizon errors in sky cover retrievals from sky images, The Open Atmos. Sci. J., 4, 45-52, doi:10.2174/1874282301004010045, 2010.

Long, C. N., and DeLuisi, J. J.: Development of an automated hemispheric sky imager for cloud fraction retrievals, in: Proceedings of the tenth Symposium on meteorological observations and instrumentation, Phoenix, AZ, Amer. Meteor. Soc., 171-174, 1998.

Long, C.N., Sabburg, J., Calbó, J., and Page‘s, D.: Retrieving cloud characteristics from ground-based daytime color all-sky images, J. Atmos. Ocean. Tech., 23, 633-652, doi:10.1175/JTECH1875.1, 2006.

Long, C., Slater, D., and Tooman, T.: Total Sky Imager (TSI) Model 880 status and testing results, Tech. Rep., DOE Office of Science Atmospheric Radiation Measurement (ARM) Program, United States, 36 pp., 2001.

Lund, I. A.: Joint probabilities of cloud-free lines of sight through the atmosphere at Grand Forks, Fargo, and Minot, North Dakota, Air Forces Surveys in Geophys., 262, 1973.

Lund, I. A., Grantham D. D., and Davis, R. E.: Estimating probabilities of cloud-free field of view from the Earth through the atmosphere, J. Appl. Meteorol., 19, 452-463, doi:10.1175/1520-0450(1980)019<0452:EPOCFF>2.0.CO;2, 1980.

Lynch, D. K. and Schwartz, P.: Intensity profile of the 22° halo, J. Opt. Soc. Am. A, 2, 584-589, doi:10.1364/JOSAA.2.000584, 1985.

Lyons, R. D.: Computation of height and velocity of clouds over Barbados from a whole-sky camera network, Issue 95 of SMRP research paper, Satellite and Mesometeorology Research Project, University of Chicago, SMRP Research Rep. 95, 18 pp, 1971.

Macke, A., Mueller, J., and Raschke, E.: Single scattering properties of atmospheric ice crystals, J. Atmos. Sci., 53, 2813-2825, doi:10.1175/1520-0469(1996)053<2813:SSPOAI>2.0.CO;2, 1996.

Martínez-Chico, M., Batlles, F. J., and Bosch, J. L.: Cloud classification in a Mediterranean location using radiation data and sky images, Energy, 36, 4055-4062, doi:10.1016/j.energy.2011.04.043, 2011.

Meeus, J. H.: Astronomical Algorithms, 2nd edition, Willmann-Bell, Richmond, VA, 477 pp., 1999.

Mishchenko, M.I., and Macke, A.: Incorporation of physical optics effects and computation of the Legendre expansion for ray-tracing phase functions involving δ-function transmission, J. Geophys. Res., 103 (D2), 1799-1805, doi:10.1029/97JD03121, 1998.

Mishchenko, M.I., and Macke, A.: How big should hexagonal ice crystals be to produce halos?, Appl. Optics, 38, 1626-1629, doi:10.1364/AO.38.001626, 1999.

Orsini, A., Tomas, C., Calzolari, F., Nardino, M., Cacciari, A., and Georgiadis, T.: Cloud cover classification through simultaneous ground-based measurements of solar and infrared radiation, Atmos. Res., 61, 251-275, doi:10.1016/S0169-8095(02)00003-0, 2002.

Pagès, D., Calbó, J., and González, J.A.: Using routine meteorological data to derive sky conditions, Ann. Geophys., 21, 649-654, doi:10.5194/angeo-21-649-2003, 2003.

Pfister, G., McKenzie, R.L., Liley, J.B., Thomas, A., Forgan, B.W., and Long, C.N.: Cloud coverage based on all-sky imaging and its impact on surface solar irradiance, J. Appl. Meteorol., 42, 1421-1434, doi:10.1175/1520-0450(2003)042<1421:CCBOAI>2.0.CO;2, 2003.

Qiu, J.: Cloud optical thickness retrievals from ground-based pyranometer measurements, J. Geophys. Res., 111, D22206, doi:10.1029/2005JD006792, 2006.

Rapp-Arraras, I., and Domingo-Santos, J. M.: Functional forms for approximating the relative optical air mass, J. Geophys. Res., 116, D24308, doi:10.1029/2011JD016706, 2011.

Ray, S. F.: Applied photographic optics, Focal Press, Oxford, 2002.

Rocks, J. K.: The microscience whole-sky sensor, Fifth Tri-Service Clouds Modelling Workshop, United States Naval Academy, Annapolis, MD, 23-24 June, 1987.

Sassen, K., Knight, N. C., Yoshihide, T., and Heymsfield, A. J.: Effects of ice-crystal structure on halo formation: cirrus cloud experimental and ray-tracing modeling studies, J. Atmos. Sci., 36, 838-851, doi:10.1175/1520-0469, 1979.

Sassen, K., Zhu, J., and Benson, S.: Midlatitude cirrus cloud climatology from the Facility for Atmospheric Remote Sensing. IV. Optical displays, Appl. Optics, 42, 332-341, doi:10.1364/AO.42.000332, 2003.

Seiz, G., Baltsavias, E. P., and Gruen, A.: Cloud mapping from the ground: Use of photogrammetric methods. Photogramm. Eng. Rem. S., 68, 941-951, doi:10.1.1.577.6011, 2002.

Shaklin, I. A., and Lund, M. D.: Photogrammetrically determined cloud-free lines-of-sight through the atmosphere, J. Appl. Meteorol., 11, 773-782, doi:10.1175/1520-0450(1972)011<0773:PDCFLO>2.0.CO;2, 1972.

Shaklin, I. A., and Lund M. D.: Universal methods for estimating cloud-free lines-of-sight through the atmosphere, J. Appl. Meteorol., 12, 28-35, doi:10.1175/1520-0450(1973)012<0028:UMFEPO>2.0.CO;2, 1973.

Shcherbakov, V., Gayet, J. F., Jourdan, O., Strom, J., and Minikin, A.: Light scattering by single ice crystals of cirrus clouds, Geophys. Res. Lett., 33, L15809, doi:10.1029/2006GL026055, 2006.

Shcherbakov, V.: Why the 46° halo is seen far less often than the 22° halo?, J. Quant. Spectrosc. Ra., 124, 37-44, doi:10.1016/j.jqsrt.2013.03.002, 2013.

Shields, J. E., Johnson, R. W., Karr, M. E., Weymouth, R.A., and Sauer, D. S.: Delivery and development of a day/night whole sky imager with enhanced angular alignment for full 24 hour cloud distribution assessment, Final Report, Marine Physical Laboratory, Scripps Institution of Oceanography, University of California, San Diego, 19 pp., 1997.

Shields, J. E., Karr, M. E., Johnson, R. W., and Burden, A. R.: Day/night whole sky imagers for 24-h cloud and sky assessment: history and overview, Appl. Optics, 52, 1605-1616, doi:10.1364/AO.52.001605, 2013.

Shields, J. E., Koehler, T. L., and Johnson, R. W.: Whole sky imager, in: Proceedings of the Cloud Impacts on DOD Operations and Systems, Marine Physical Laboratory, Scripps Institution of Oceanography, University of California, San Diego, 123-128, 1989/90.

Slater, D. W., Long, C. N., and Tooman, T. P.: Total sky imager/whole sky imager cloud fraction comparison, in: Proceedings of the Eleventh ARM Science Team Meeting, Atlanta, Georgia, 19-23 March 2001, 1-11, 2001.

Smith, H. R., Connolly, P. J., Baran, A. J., Hesse, E., Smedley, A. R., and Webb, A. R.: Cloud chamber laboratory investigations into scattering properties of hollow ice particles, J. Quant. Spectrosc. Ra., 157, 106-118, doi:10.1016/j.jqsrt.2015.02.015, 2015.

Tapakis, R., and Charalambides, A. G.: Equipment and methodologies for cloud detection and classification: A review, Sol. Energy, 95, 392-430, doi:10.1016/j.solener.2012.11.015, 2013.

Ulanowski, Z. J.: Ice analog halos, Appl. Optics, 44, 5754-5758, doi:10.1016/j.jqsrt.2005.11.052, 2005.

Ulanowski, Z. J., Hesse, E., Kaye, P., and Baran, A. J.: Light scattering by complex ice-analogue crystals, J. Quant. Spectrosc. Ra., 100, 382-392, doi:10.1016/j.jqsrt.2005.11.052, 2006.

Ulanowski, Z. J., Kaye, P. H., Hirst, E., Greenaway, R. S., Cotton, R. J., Hesse, E., and Collier, C. T.: Incidence of rough and irregular atmospheric ice particles from Small Ice Detector 3 measurements, Atmos. Chem. Phys.,13, 1649-1662, doi:10.5194/acp-14-1649-2014, 2014.

Um, J., and McFarquhar, G. M.: Dependence of the single scattering properties of small ice crystals on idealized shape models, Atmos. Chem. Phys., 10, 28109-28149, doi:10.5194/acp-11-3159-2011, 2010.

Yi, B., Yang, P., Baum, B. A., L'Ecuyer, T., Oreopoulos, L., Mlawer, E. J., Heymsfield, A. J., and Liou, K. N.: Influence of Ice Particle Surface Roughening on the Global Cloud Radiative Effect, J. Atmos. Sci., 70, 2794-2807, doi:10.1175/JAS-D-13-020.1,35 2013.

Figure 1. All-sky daytime camera with occulting disk in operation in the foreground. The night time camera is in the background and the right.

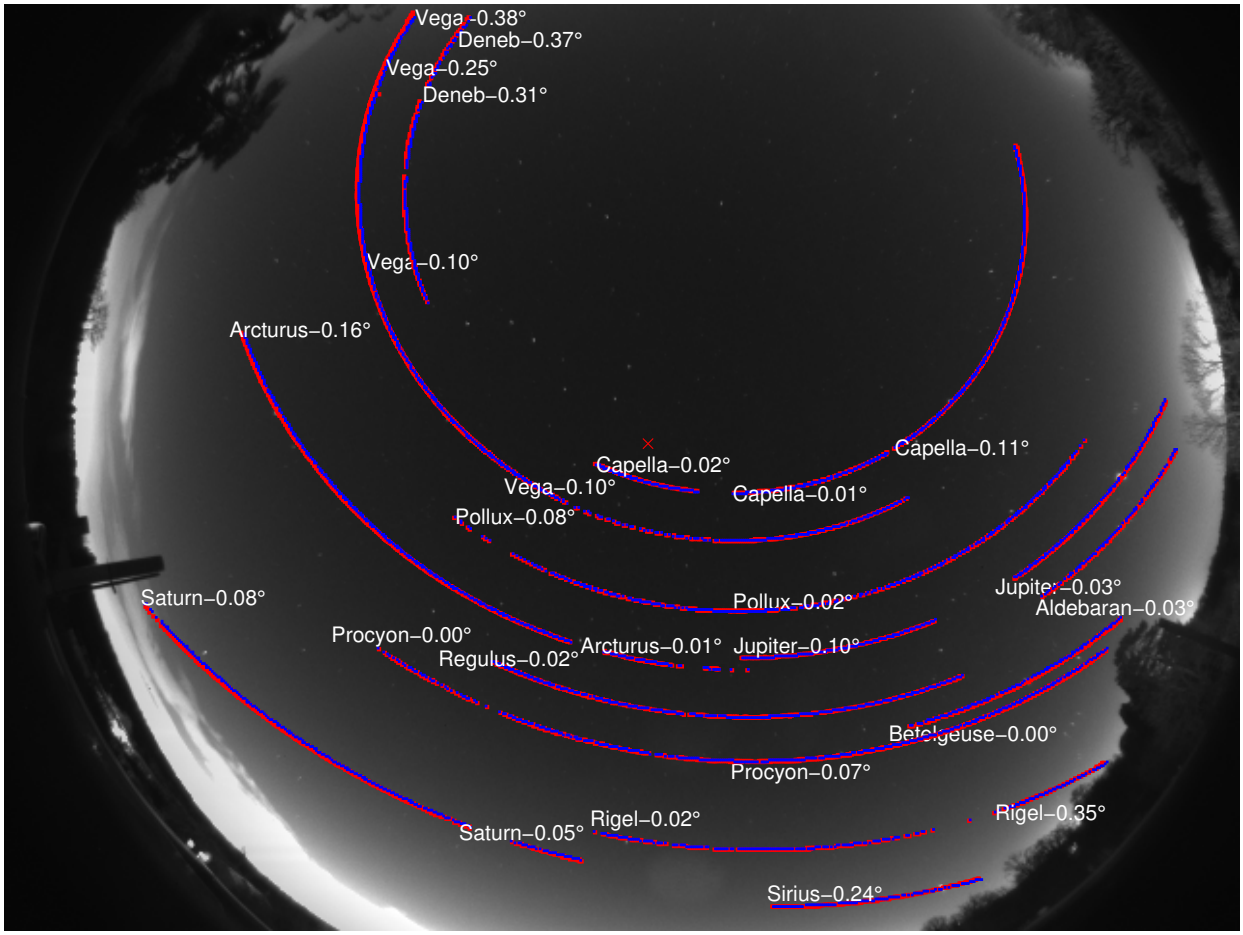

Figure 2. Predicted (blue dots, from Eq. (1) and (2)) and actual (red dots) star and planet trajectories. Each trajectory is labelled with the name of the star-planet and the mean angular difference between predicted and actual positions.

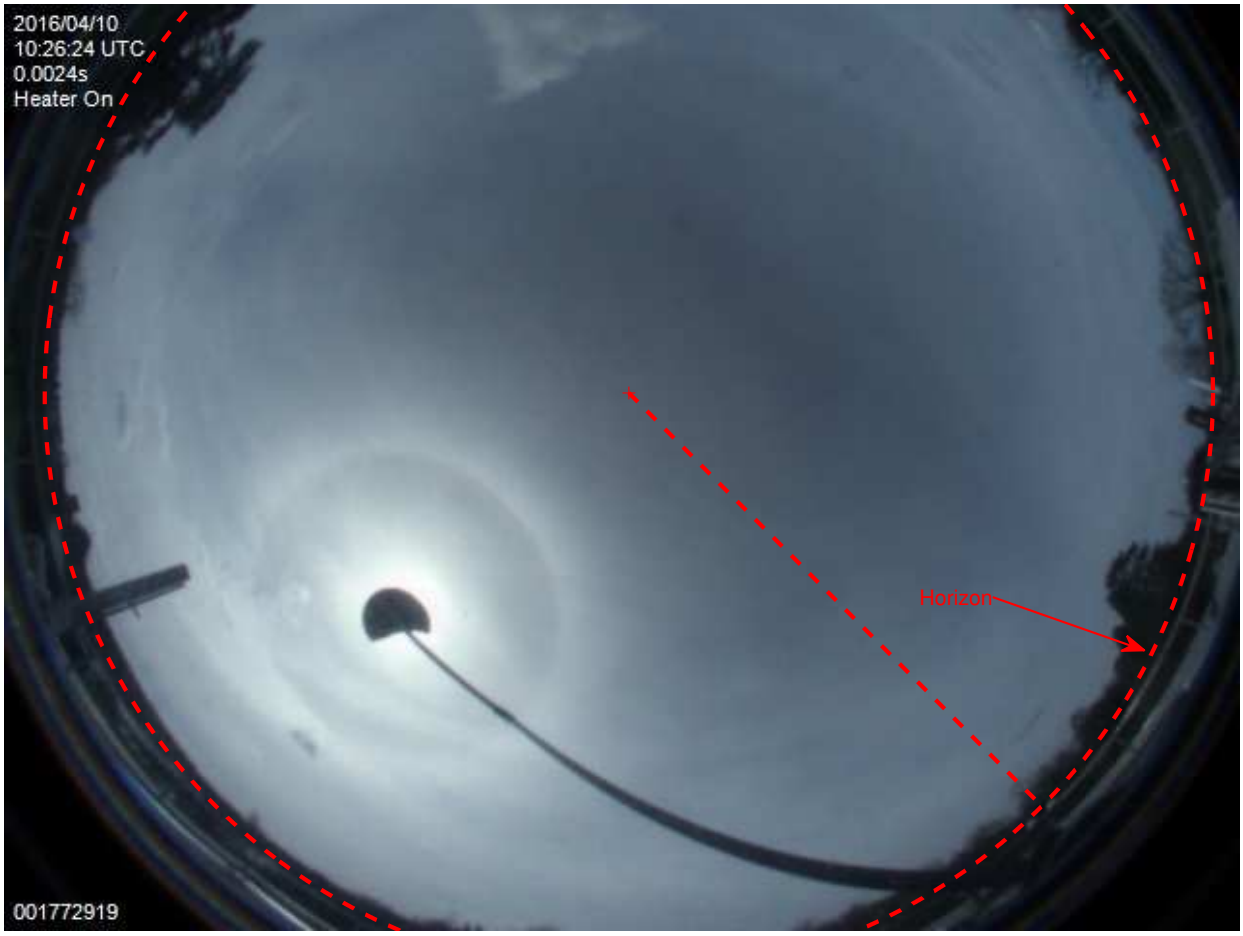

Figure 3. All-sky daytime camera image obtained on the 10th of April 2016 at 10:26 am showing horizon (red solid circle).

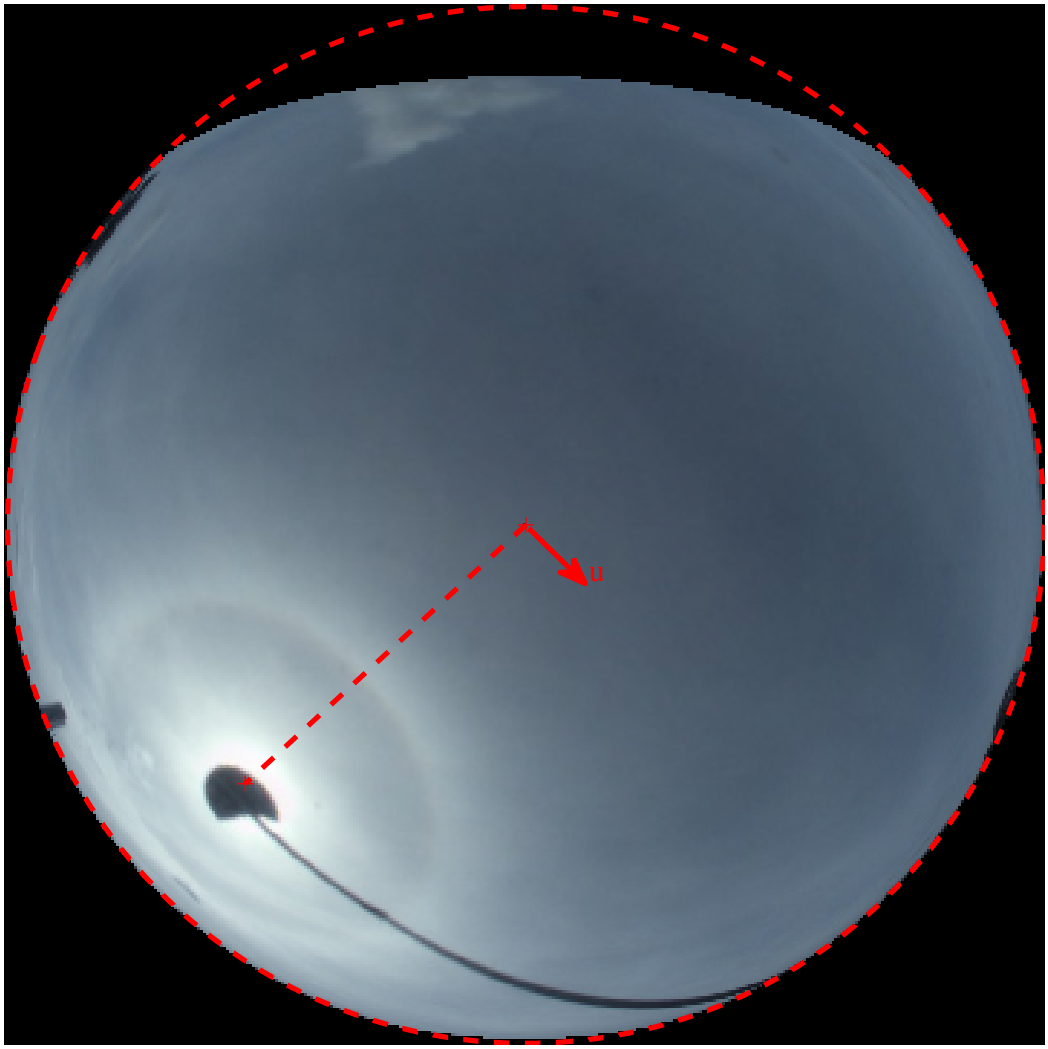

Figure 4. Projection of the original image from Fig. 3 onto a sphere (upper hemisphere).

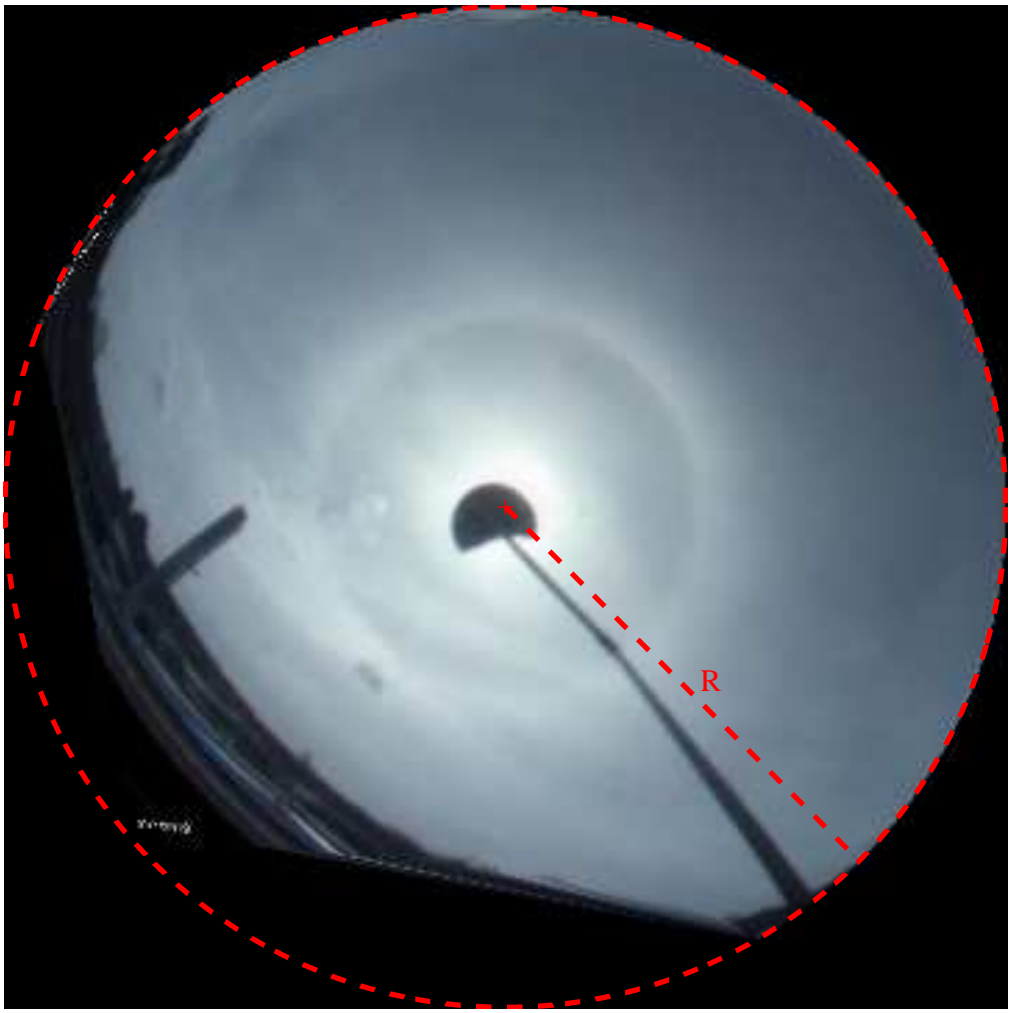

Figure 5. Image from Fig. 4 after rotation (upper hemisphere only).

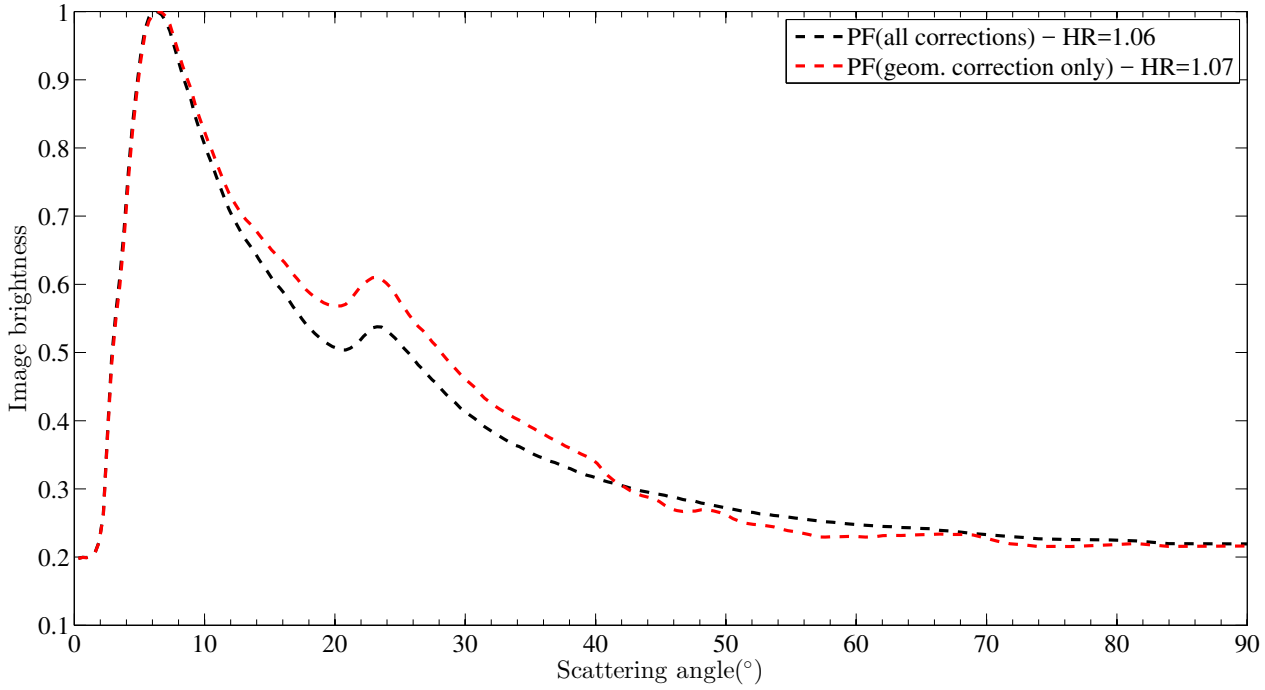

Figure 6. Measured scattering phase function corresponding to image in Fig. 3 with geometric correction only - red-dashed, with geometric, air mass, mask and vignetting corrections - black-dashed. The corresponding HR measures are also shown.

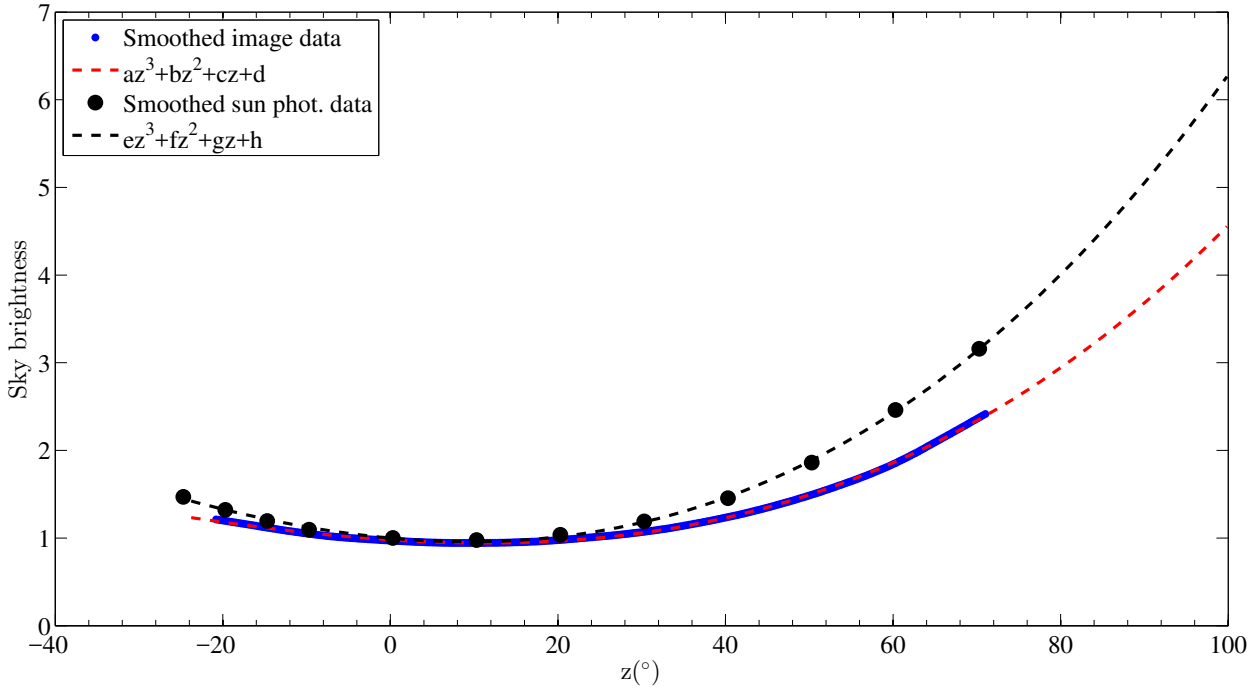

Figure 7. All-sky camera and sun photometer normalized fitting polynomials (black-dashed line - Sun photometer, red-dashed line - Camera).

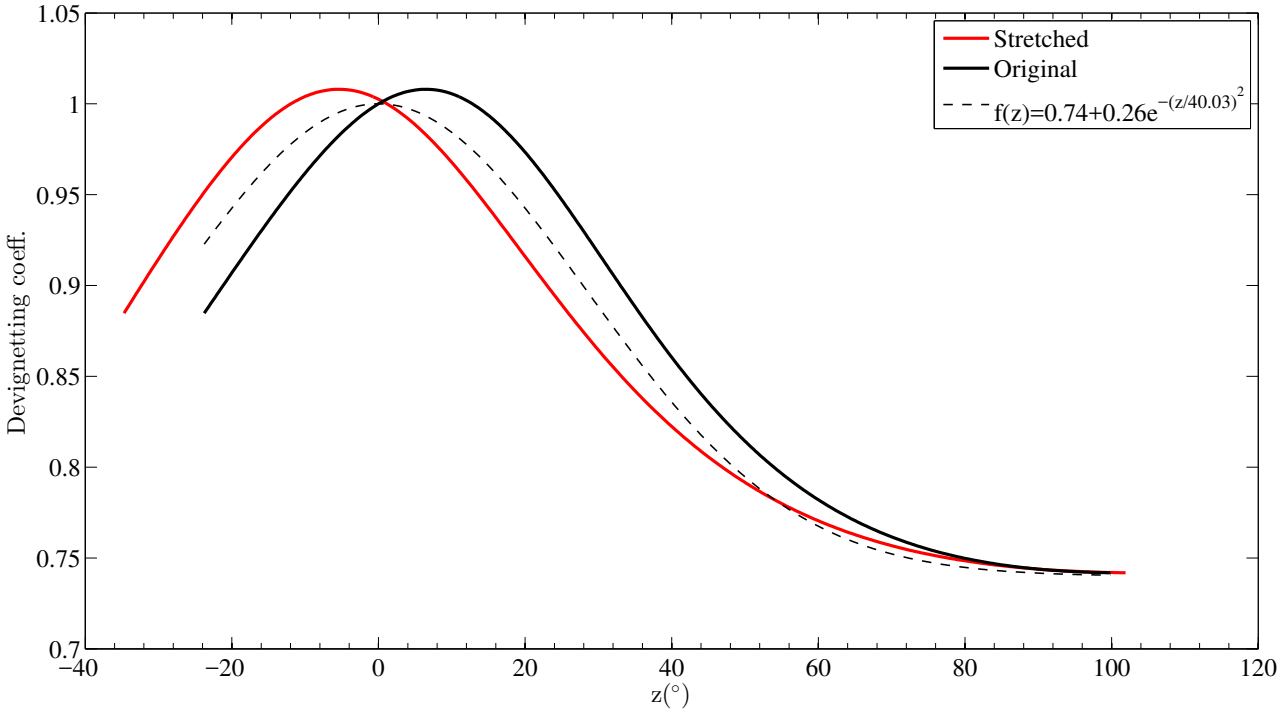

Figure 8. Devignetting coefficient: black line: original data, red line: stretched curve, dashed line: fit.

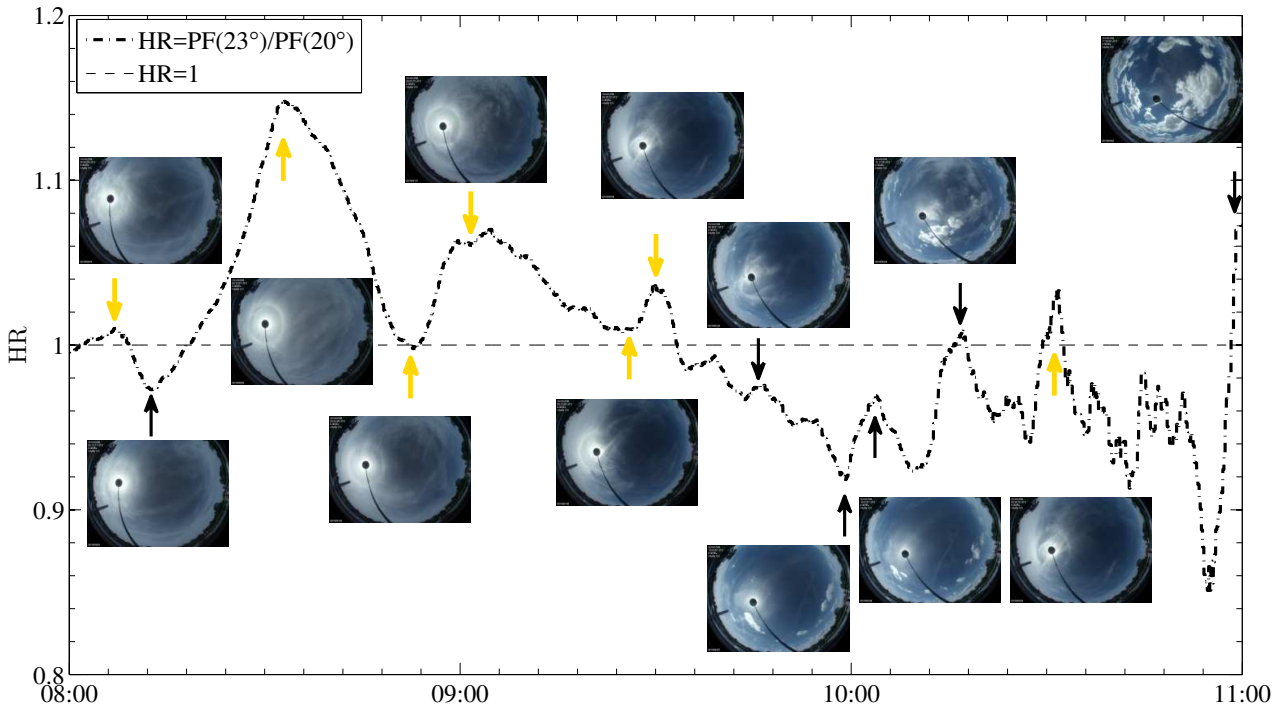

Figure 9. HR time series from 6th July 2016 between 8 am and 11 am. All-sky images corresponding to peaks and dips are also shown. Yellow arrows indicate presence of relatively bright halo while black ones indicate either presence of faint halo or absence of it.

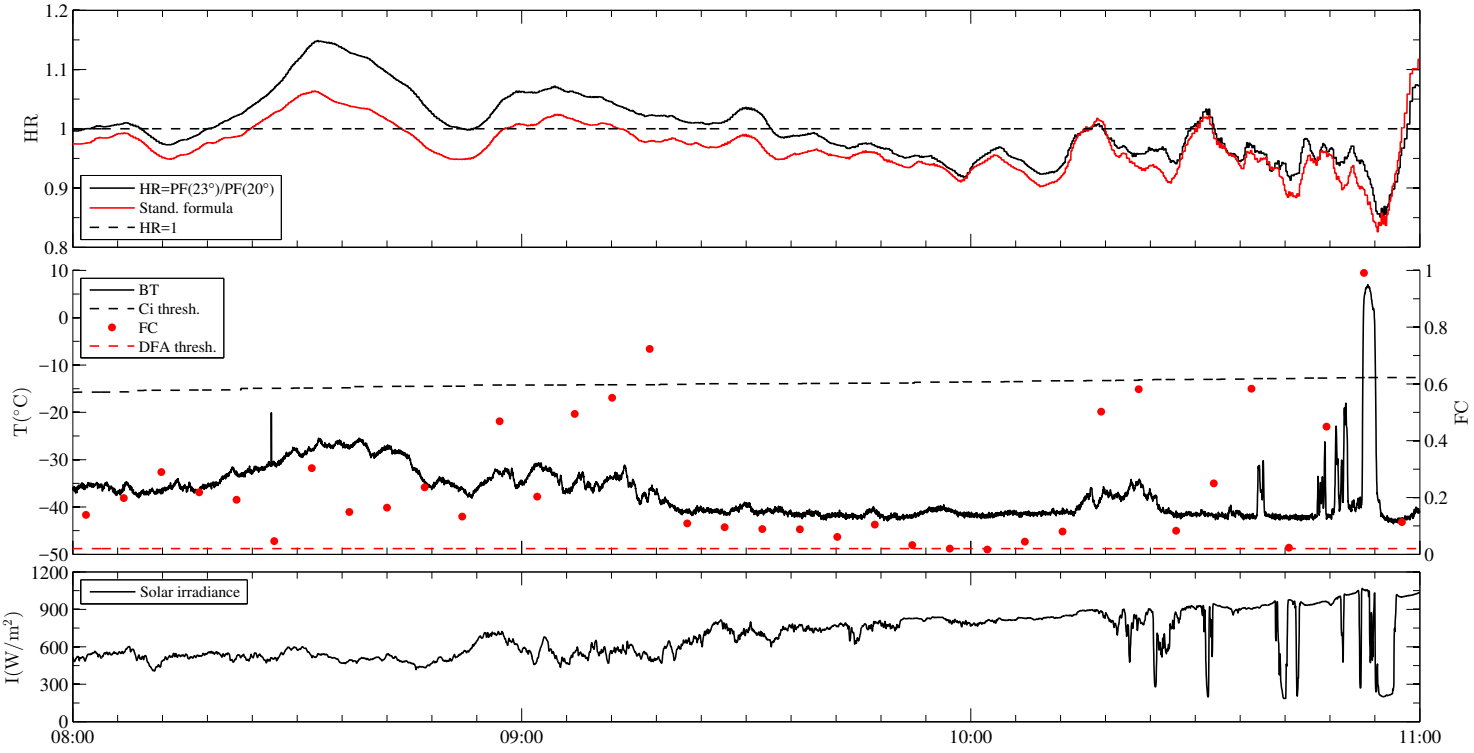

Figure 10. Time series from 6th July 2016 between 8 am and 11 am. Top plot: HR, black line - new definition, red line - standard formula - (see text); middle plot: BT - black line, FC - red dot, DFA threshold - red-dashed line, Ci threshold - black-dashed line; bottom plot: solar irradiance.

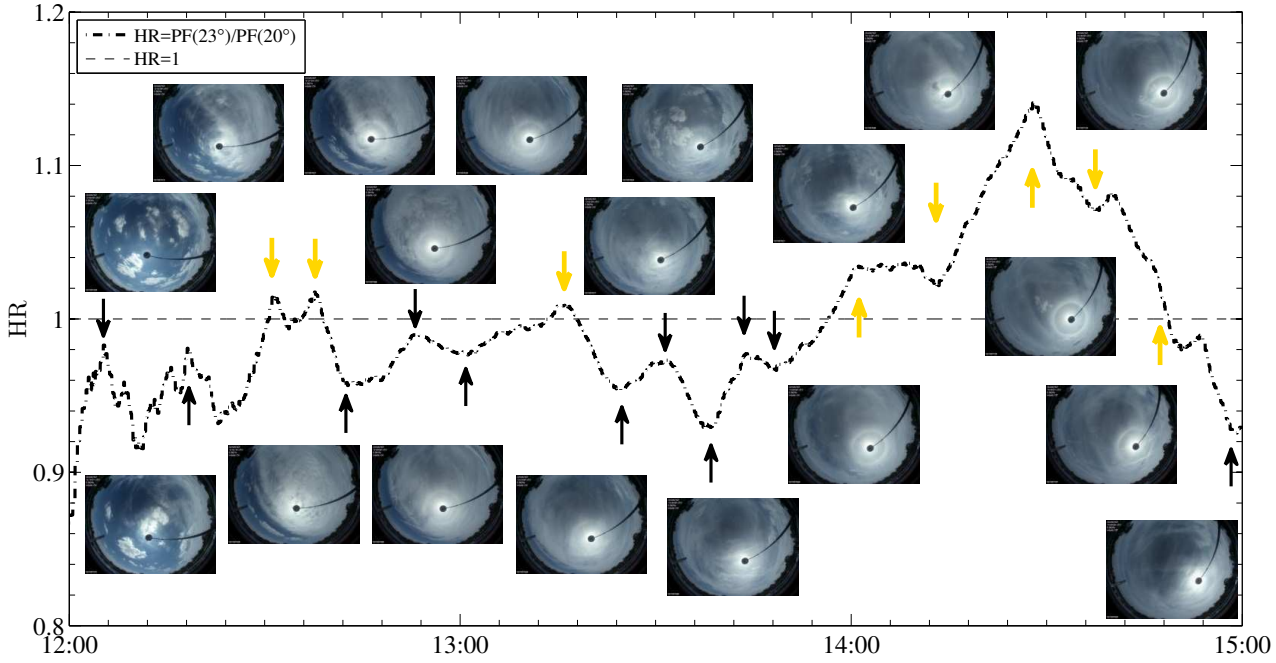

Figure 11. As Fig. 9, but HR time series from 7th July 2016 between 12 noon and 3pm.

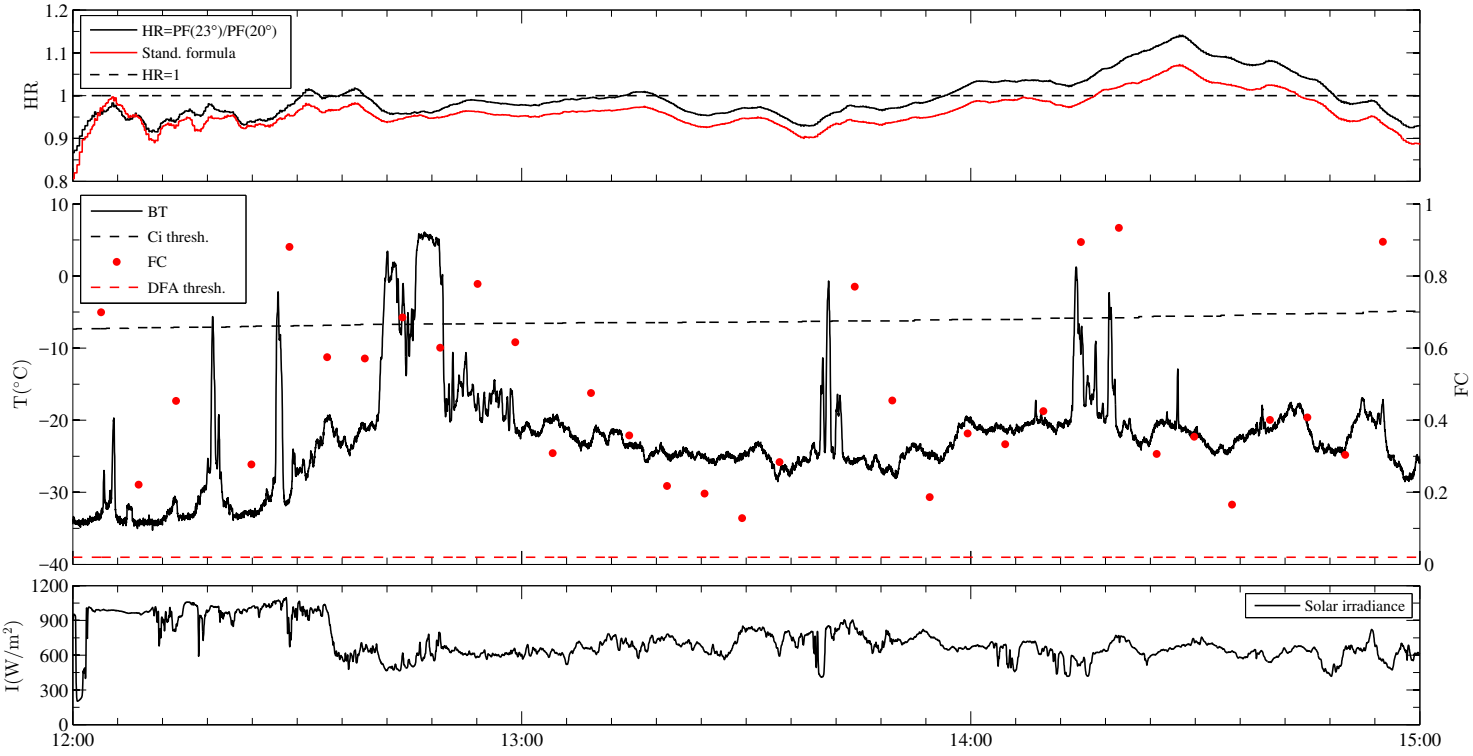

Figure 12. Time series from 7th July 2016 between 12 noon and 3 pm. Top plot: HR, black line - new definition, red line - standard formula - (see text); middle plot: BT - black line, FC - red dot, DFA threshold - red-dashed line, Ci threshold - black-dashed line; bottom plot: solar irradiance.